Microstrip Antennas:
Broadband Radiation Patterns
Using Photonic Crystal Substrates

By

Keith C. Huie

Thesis submitted to the Faculty of the
Virginia Polytechnic Institute and State University
in partial fulfillment of the requirements for the degree of

Master of Science
in
Electrical Engineering

Dr. Richard Claus, Chairman
Dr. Ravi Saraf
Dr. Warren Stutzman

January 11, 2002
Blacksburg, VA

Keywords: Microstrip Antenna, Surface Waves, Photonic Crystals, Bandgap, Broadband

Microstrip Antennas: Broadband Radiation Patterns
Using Photonic Crystal Substrates

Keith Huie

(ABSTRACT)

The purpose of this thesis is to investigate a novel method to develop broadband microstrip (patch) antennas using substrates containing photonic crystals. Photonic crystals are a class of periodic dielectric, metallic, or composite structures that when introduced to an electromagnetic signal can exhibit a forbidden band of frequencies (or bandgap) in which the incident signal destructively interferes and thus is unable to propagate. It is proposed that such photonic crystals will reduce surface waves and prohibit the formation of substrate modes, which are commonly known inhibitors of patch antenna designs. By reducing or eliminating the effects of these electromagnetic inhibitors with photonic crystals, a broadband response can be obtained from inherently narrowband antennas. In addition, it is also proposed that the behavior of the photonic crystals will lead to a reduction in pattern sidelobes resulting in improvements in radiation pattern front-to-back ratio and overall antenna efficiency. This research is verified through analytical simulations and experimental investigations in the Virginia Tech anaechoic chamber.

Acknowledgments

First of all, I would like to thank my wife, Jean, for all her love and support through my studies. She has inspired me in many ways ever since the day we first met in Pittsburgh. Our three years of marriage have been the most joyous experience in my life and I look forward to many more years together. Love you Baby.

I would like to thank my advisor, Dr. Richard O. Claus, for all of his constant support, motivation, and friendship throughout the completion of this thesis. It has been an absolute privilege to work for him for the past two years and I look forward to our future endeavors as I continue my studies towards a PH.D. Thanks also to Dr. Warren Stutzman and Dr. Ravi Saraf for their assistance in this research and in my professional development in general.

In addition, thanks to my fellow lab members and business associates for their encouragement and friendship during the past two years. Thanks to Mike Barts and Randall Nealy for their expertise and assistance in taking antenna measurements in the Antenna Labs.

Finally, I would like to give special thanks my parents and brother who has always been there went I needed with constant support and guidance. Love you guys.

Table of Contents

Table of Figures

Chapter 1: Thesis Overview

1.1 Introduction

In recent years, the current trend in commercial and government communication systems has been to develop low cost, minimal weight, low profile antennas that are capable of maintaining high performance over a large spectrum of frequencies. This technological trend has focused much effort into the design of microstrip (patch) antennas. With a simple geometry, patch antennas offer many advantages not commonly exhibited in other antenna configurations. For example, they are extremely low profile, lightweight, simple and inexpensive to fabricate using modern day printed circuit board technology, compatible with microwave and millimeter-wave integrated circuits (MMIC), and have the ability to conform to planar and non-planar surfaces. In addition, once the shape and operating mode of the patch are selected, designs become very versatile in terms of operating frequency, polarization, pattern, and impedance. The variety in design that is possible with microstrip antennas probably exceeds that of any other type of antenna element [1].

1.2 Thesis Motivation

Despite the many advantages of patch antennas, they do have some considerable drawbacks. One of the main limitations with patch antennas is their inherently narrowband performance due to its resonant nature. With bandwidths as low as a few percent[2], broadband applications using conventional patch designs are limited. Other characteristics of patch antennas include low efficiencies, limited power capacity,

[1] Brown and McMahon, "Large Electromagnetic Stop Bands in Metallo-Dielectric Photonic Crystals," *Applied Physics Letters*, vol. 67, 1995

[2] Stutzman and Thiele, *Antenna Theory and Design*, 2nd ed: John Wiley & Sons, Inc., 1998.

spurious feed radiation, poor polarization purity, and manufacturing tolerance problems[3].

For over two decades, research scientists have developed several methods to increase the bandwidth of a patch antenna. Many of these techniques involve adjusting the placement and/or type of element used to feed (or excite) the antenna. The simplest and most direct approach is to increase the thickness of the substrate, while using a low dielectric substrate[3]. This can extend efficiency (as much as 90% if the surface waves are not included) and bandwidth (up to 35%)[4]. However, surface waves must be included, since surface waves extract power from the direct radiation pattern, resulting in increased sidelobe levels, antenna loss, and a decrease in efficiency. Moreover, as will be explained in Chapter 2, the probability of surface wave formation increases as the thickness of the substrate increases.

As a patch antenna radiates, a portion of the total available power for direct radiation becomes trapped along the surface of the substrate. This trapped electromagnetic energy leads to the development of surface waves[5]. In fact, the ratio of power that radiates into the substrate compared to the power that radiates into air is approximately ($\varepsilon^{3/2}$:1)[5]. This is governed by the rules of total internal reflection, which state that any field line radiated into the substrate at angles greater than the critical angle ($q_c = \sin^{-1}(e^{-1/2})$) are totally internally reflected at the top and bottom surfaces. This is illustrated in Figure 1. Therefore, for a substrate with dielectric constant ε = 10.2, nearly $1/3$ of the total radiated power is trapped in the substrate with a critical angle of roughly 18.2 degrees.

---

[3] Pozar and Schaubert, "Microstrip Antennas," *Proceedings of the IEEE*, vol. 80, 1992

[4] Balanis, *Antenna Theory Analysis and Design*, 2nd ed: John Wiley & Sons, Inc., 1997.

[5] Brown and Parker, "Radiation Properties of a Planar Antenna on a Photonic-Crystal Substrate," *J Opt Soc Am B*, vol. 10, 1993

Surface wave effects can be eliminated by using cavities or stacked substrate techniques[6]. However, this has the fundamental drawback of increasing the weight, thickness, and complexity of the microstrip antenna, thus negating many of the advantages of using microstrip antennas. These complications and others prevent microstrip antennas from becoming the standard in the microwave telecommunications community.

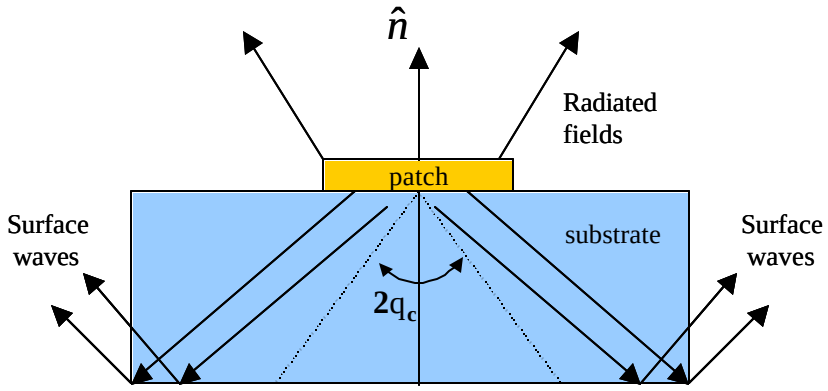

Figure 1. Field lines radiating from a patch antenna; illustrates the formation of surface waves

A recently developed method for improving the bandwidth and efficiency of a patch antenna is the insertion of a photonic crystal array into the substrate. Photonic crystals are a class of periodic dielectric, metallic, or composite structures that when introduced to an electromagnetic signal can exhibit a forbidden band of frequencies (or bandgap) in which the incident signal destructively interferes and thus is unable to propagate. It is proposed that if photonic crystals are inserted into the substrate of a patch antenna, then a broadband response can be obtained from this inherently narrowband antenna. This will result in improvements in the radiation characteristics of the patch antenna, by reducing pattern sidelobes and improving front-to-back pattern ratios and overall efficiency. This research has been verified through analytical simulations and experimental investigations in the Virginia Tech (VT) anechoic chamber.

---

[6] Brown and Parker, "Radiation Properties of a Planar Antenna on a Photonic-Crystal Substrate," *J Opt Soc Am B*, vol. 10, 1993

1.3 Thesis Outline

The outline of this thesis is organized as follows: Chapter 2 provides a brief technical description of microstrip antennas focusing on basis characteristics and typical excitation (feeding) methods, and concludes with an analytical model of a patch. Chapter 3 describes the underlying principles of photonic crystals and their associated bandgaps. This topic extends into Chapter 4, where the electromagnetic evaluation of the bandgap is discussed. Chapter 4 concludes with a brief summary of how photonic crystals have been used in the development of thick and thin substrate microstrip antennas, and with the introduction of a novel approach to designing patch antennas with photonic crystals. Chapter 5 describes the software packages used to analytically evaluate the antennas and to determine the location and extend of the bandgaps for the photonic crystals. Chapter 6 gives an overview of the antenna design methodology. Chapter 7 illustrates the antenna fabrication process. Chapter 8 describes the experimental analysis and results of evaluation using the measurement equipment at the VT Antenna Lab. Chapter 9 summaries the results and discusses possible applications and tradeoffs when using photonic crystals with antennas.

Chapter 2: Microstrip Antennas

The microstrip antenna was first introduced in the 1950's, but it was not until the 1970's and the development of printed-circuit technology[7,8] that serious advancements in this research area had begun. Through decades of research, it was identified that the performance and operation of a microstrip antenna is driven mainly by the geometry of the printed patch and the material characteristics of the substrate onto which the antenna is printed. Therefore, it is conceivable that with proper manipulations to the substrate, i.e. the inclusion of photonic crystals, improved antenna performance can result. As stated by R.C. Hansen (IEEE Fellow, 18 Sept 98), "there is little improvement to be realized in the arrangement of wires in the antenna; a significant improvement will come from the use of new materials." The following sections discuss the fundamental parameters and manufacturing requirements associated with the design of microstrip antennas.

2.1 Basic Characteristics

As shown in Figure 2, conventional microstrip antennas consist of a pair of parallel conducting layers separating a dielectric medium, referred to as the substrate. In this configuration, the upper conducting layer or "patch" is the source of radiation where electromagnetic energy fringes off the edges of the patch and into the substrate. The lower conducting layer acts as a perfectly reflecting ground plane, bouncing energy back through the substrate and into free space. Although similar in operation to a microstrip transmission line, the patch antenna is much larger in volume providing a distinct contrast between the two. Physically, the patch is a thin conductor that is an

[7] Balanis, *Antenna Theory Analysis and Design*, 2nd ed: John Wiley & Sons, Inc., 1997.
[8] Pozar and Schaubert, "Microstrip Antennas," *Proceedings of the IEEE*, vol. 80, 1992

appreciable fraction of a wavelength in extent, parallel to a ground plane and a small fraction of a wavelength above the ground plane [9]. In most practical applications, patch antennas are rectangular or circular in shape[10], however, in general, any geometry is possible.

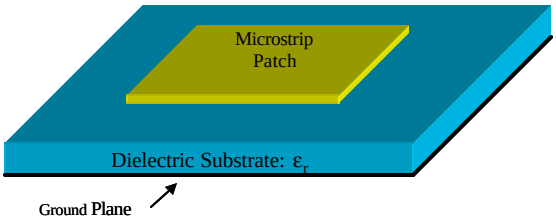

Figure 2. Typical geometry of a microstrip antenna

Commercial substrate materials are readily available for use at RF and microwave frequencies, specifically for the design of microstrip antennas and printed circuits. Selection is based on desired material characteristics for optimal performance over specific frequency ranges. Common manufacturer specifications include dielectric constant, dissipation factor (loss tangent), thickness, and Young's modulus. Values for dielectric constants range from $2.2 = \varepsilon_r = 12$ for operation at frequencies ranging from 1 to 100 GHz[11,12].

The thickness of the substrate is of considerable importance when designing microstrip antennas. The most desirable substrates for antenna performance are the ones that are thick with a low dielectric constant[10]. This tends to result in an antenna with a large bandwidth and high efficiency due to the loosely bound fringing fields that emanate from the patch and propagate into the substrate. However, this comes at the expense of a large volume antenna and an increased probability of surface wave formation. On the other hand, thin substrates with high dielectric constants reduce the overall size of the

[9] Stutzman and Thiele, *Antenna Theory and Design*, 2nd ed: John Wiley & Sons, Inc., 1998.
[10] Pozar and Schaubert, "Microstrip Antennas," *Proceedings of the IEEE*, vol. 80, 1992
[11] Balanis, *Antenna Theory Analysis and Design*, 2nd ed: John Wiley & Sons, Inc., 1997.
[12] Stutzman and Thiele, *Antenna Theory and Design*, 2nd ed: John Wiley & Sons, Inc., 1998.

antenna and are compatible with MMIC devices, since the fringing fields are tightly bound to the substrate. With thin substrates, coupling and electromagnetic interference (EMI) issues are less probable. However, because of the relatively higher loss tangents (dissipation factors), they are less efficient and have relatively smaller bandwidths[13]. Therefore, there is a fundamental tradeoff that must be evaluated in the initial stages of the microstrip antenna design - to obtain loosely bound fields to radiate into free space while keeping the fields tightly bound for the feeding circuitry and to avoid EMI.

2.2 Feeding Methods

There are several techniques available to feed or transmit electromagnetic energy to a microstrip antenna. The most popular methods are the microstrip transmission line, coaxial probe, aperture coupling, and proximity coupling[13],[14],[15]. Figure 3 illustrates each of these configurations; corresponding equivalent circuits are shown in Figure 4. In each of the equivalent circuits, an RLC circuit symbolizes the patch, illustrating its resonant nature. The resistance (R) corresponds to loss associated with the conductors (ground plane and patch) and substrate (loss tangent).

The simplest feeding methods to realize are those of the coaxial probe and microstrip transmission line, illustrated in Figures 3a and 3b and symbolized in Figures 4a and 4b. Both approaches utilize direct contact with the patch to induce excitation. The point of excitation (contact point) is adjustable, enabling the designer to control the impedance match between feed and antenna, polarization, mode of operation, and excitation frequency. Generally, for direct contact feeds, the best impedance match is obtained when the contact point is off-centered. This produces asymmetries in the patch

---

[13] Balanis, *Antenna Theory Analysis and Design*, 2nd ed: John Wiley & Sons, Inc., 1997.
[14] Pozar and Schaubert, *Microstrip Antenna: The Analysis and Design of Microstrip Antennas and Arrays*: IEEE Press, 1995.
[15] Pozar and Schaubert, "Microstrip Antennas," *Proceedings of the IEEE*, vol. 80, 1992

excitation, which generate higher order modes[13]. These higher order modes induce a cross-polarized component in the principal plane antenna patterns, which draw power from the dominant TM_{010} mode and results in degradation of the antenna's main beam. Therefore, oftentimes, a trial-and-error approach is used to obtain the optimum match for the direct contact feeds.

Another disadvantage of the direct contact feeds is that they are inherently narrowband devices. These feeds, whether coaxial or microstrip, are "matched" to specific impedances (in most cases 50Ω) for a select range of frequencies. Operation outside this range automatically degrades antenna performance due to the inherent mismatch between the antenna and the feed.

To overcome some of the shortcomings of the direct-coupled feeds, a variety of "non-contacting coupled feeds" has been developed. The two main configurations are the aperture-coupled (Figures 3c and 4c) and proximity-coupled (Figure 3d and 4d) feeds. The aperture-coupled configuration consists of two parallel substrates separated by a ground plane. Excitation of the patch is accomplished by coupling energy from a microstrip line through a small aperture in the ground plane. With this arrangement, the microstrip feed is designed on a thin-high dielectric constant substrate, which tightly binds the field lines, while the patch is designed on a thick-low dielectric constant substrate. The ground plane isolates the feed from the patch, and thus minimizes spurious radiation from the feed, which would interfere with the antenna pattern[16]. Therefore, the design of the patch and the transmission line are independent. In contrast, the proximity-coupled technique operates in a manner similar to that of the aperture-coupled configuration except the ground plane is removed. Both non-contacting feeds have similar advantages with the exception that the thickness changes with removal of the ground plane.

---

[16] Pozar and Schaubert, "Microstrip Antennas," *Proceedings of the IEEE*, vol. 80, 1992

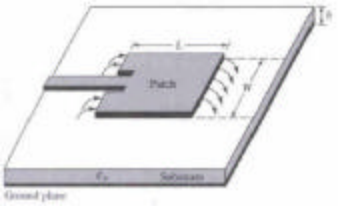	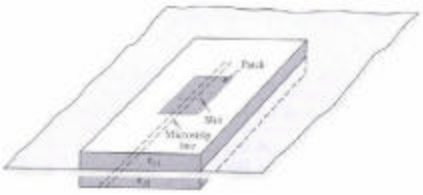
(3a) Microstrip line configuration using a direct contact approach	(3c) Aperture coupled configuration using a non-contacting approach
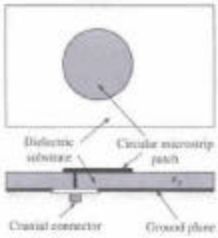	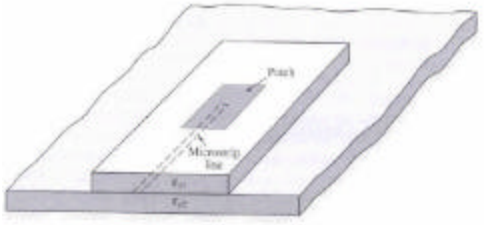
(3c) Probe fed configuration using a direct contact approach	(3d) Proximity coupled configuration using a non-contacting approach

Figure 3. Typical feeding methods used to excite a microstrip patch antenna[17]

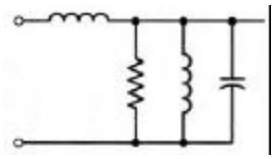	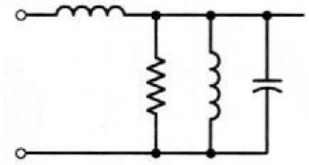	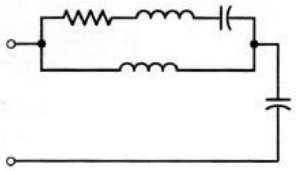	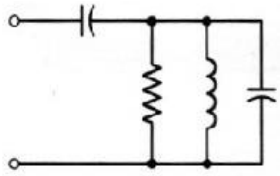
(4a) Microstrip Transmission Line	(4b) Coaxial Probe	(4c) Aperture Coupled	(4d) Proximity Coupled

Figure 4. Equivalent circuits for feeds configurations shown in Figure 3[17]

In both non-contacting configurations, there is an undesirable increase in the overall thickness of the antenna. Therefore, to reduce the complexity and size of the antennas involved in this research, it was decided to **design the structures on a thin-high dielectric constant substrate using a coaxial probe feed**. The microstrip transmission line feed was eliminated from consideration because of the design complexities associated with incorporating photonic crystals into the substrate, as will be discussed in ***Chapter 4***. Indeed, there are significant drawbacks to using the coaxial probe

[17] Pozar and Schaubert, "Microstrip Antennas," *Proceedings of the IEEE*, vol. 80, 1992

approach, but as will be discussed a substantial benefit is obtained when using them to feed a patch antenna designed with photonic crystals in the substrate.

2.3 Analytical Evaluation of a Patch Antenna

In common practice, microstrip antennas are evaluated using one of three synthesis methods – the transmission line model, the cavity model, or the full-wave model[18]. Since the inception of these techniques, several complex analytical models have been developed that account for fringing effects, special geometries, complex substrates, and mutual coupling from neighboring elements in an array. The most direct approach to evaluate patch antennas with reasonably accurate results is to use the cavity model.

In the cavity model, a patch antenna is represented as a dielectric loaded cavity. The cavity is formed via a substrate that is truncated on the top and bottom by two perfectly conducting electric boundaries – the patch and ground plane. The sidewalls are perfectly conducting magnetic boundaries that are determined by the dimensions of the patch. Therefore, the electric field lines contain within the substrate (between the patch and ground plane) are propagate perpendicular to the conducting walls, as required by Maxwell's Equations.

Using these boundary conditions, the dielectric loaded cavity can be evaluated via Huygens' equivalence principle. The equivalence principle works such that fictitious equivalent sources may be envisioned to replace the actual source of radiation, which in this case is an antenna. These fictitious sources are said to be equivalent within a region because they produce the same fields within that region as the antenna itself[18]. Huygens' principle is based on the uniqueness theorem, which states that a solution that satisfies a differential equation (e.g. Maxwell's equations) and the boundary

[18] Balanis, *Antenna Theory Analysis and Design*, 2nd ed: John Wiley & Sons, Inc., 1997.

conditions is unique[19]. In the case of a patch antenna, equivalent electric current densities $\mathbf{J_t}$ and $\mathbf{J_B}$ are formed on the top and bottom surfaces of the patch, respectively. The four sidewalls of the cavity are represented via equivalent electric and magnetic current densities. These equivalent currents are illustrated in Figure 5a and are written in general as

$$\vec{J}_s = \hat{n} \times \vec{H}_z \qquad (1)$$

$$\vec{M}_s = -\hat{n} \times \vec{E}_z \qquad (2)$$

where E_a and H_a represent the electric and magnetic fields along the walls of the cavity, respectively.

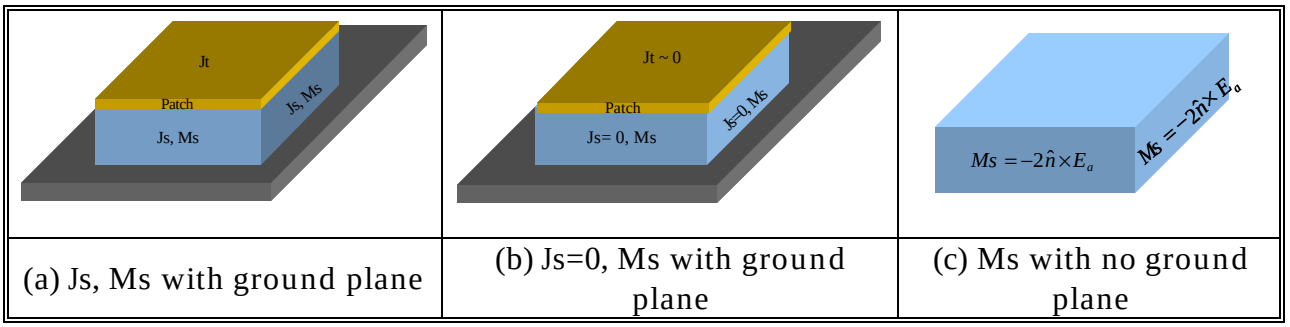

(a) Js, Ms with ground plane	(b) Js=0, Ms with ground plane	(c) Ms with no ground plane

Figure 5. Equivalent current densities on four sides of a rectangular patch antenna as specified using the Cavity Model[20]

In most practical patch designs, the substrate height-to-patch width ratio is very small, thus allowing only a small amount of current to flow to the top surface[20]. As a result, J_t is approximately zero. This ideally would not create any tangential magnetic field components (H_a) to the edges of the patch. Therefore, the equivalent electric current densities along the sidewalls are essentially zero, as illustrated in Figure 5b. The only nonzero current density is the equivalent magnetic current density (M_s) along the sidewalls of the cavity. To simplify the model, image theory is used to account for the ground plane such that the equivalent magnetic current density becomes

[19] Stutzman and Thiele, *Antenna Theory and Design*, 2nd ed: John Wiley & Sons, Inc., 1998.
[20] Balanis, *Antenna Theory Analysis and Design*, 2nd ed: John Wiley & Sons, Inc., 1997.

$$\vec{M}_s = -2\hat{n}\times\vec{E}_z \text{, as shown in Figure 5c.} \qquad (3)$$

This reduced model is similar to a cavity with four apertures or "slots" where radiation can occur. However, the equivalent current densities of length *L* and height *h* cancel, since they are equal magnitude and 180 degrees out of phase. Thus, these two sidewalls are referred to as nonradiating slots[21]. Figure 6 illustrates this cancellation effect pictorially for the dominant TM_{010} mode, assuming that $L \sim \frac{l_d}{2}$[21]. Therefore, only two slots radiate, each of width W and height h, are both equal in magnitude and phase, as shown in Figure 7. These components will thus add in phase, in a direction normal to the patch.

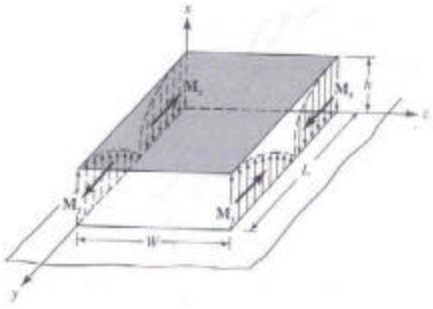

Figure 6. Current densities of non-radiating slots of a rectangular patch antenna[21]

Using Aperture Theory, an approximate formula for the radiated fields from a rectangular patch antenna can be derived. For this analysis, the E-field is assumed to be uniformly distributed along the patch with amplitude $E_{ax} = E_o$. Based on this theory, a uniform source radiating in the yz-plane can be evaluated using[22]

$$P_x = \iint_{Sa} E_{ax}(y', z') e^{jb\left(y'\sin\theta\cos\phi + z'\cos\theta\right)} dy'\, dz' \qquad (4)$$

[21] Balanis, *Antenna Theory Analysis and Design*, 2nd ed: John Wiley & Sons, Inc., 1997.
[22] Stutzman and Thiele, *Antenna Theory and Design*, 2nd ed: John Wiley & Sons, Inc., 1998.

$$E_q = jb\frac{e^{-jbr}}{2pr}(P_x \cos f) \quad (5)$$

$$E_f = jb\frac{e^{-jbr}}{2pr}\cos q(-P_x \sin f) \quad (6)$$

Equation (4) reduces to

$$P_x = E_o \frac{\sin(Y)}{Y}\frac{\sin(Z)}{Z} \quad (7)$$

$$Y = \frac{bW}{2}\sin q \sin f \quad (8)$$

$$Z = \frac{bh}{2}\cos q \quad (9)$$

For very thin substrates ($\beta h << 1$) and as the limit of $Z \rightarrow 0$, equation (7) reduces to

$$P_x = E_o \frac{\sin(Y)}{Y} \quad (10)$$

This expression is valid for only a single radiating slot. The expression when both slots radiate simultaneous is calculated using array theory. The normalized array factor for two elements, of the same magnitude and phase, separated by a distance L along the x-axis is

$$AF(q,f) = \cos(\frac{bL}{2}\sin q \cos f) \quad (11)$$

The far-field expression for a patch are evaluated from equations (5) and (6) to produce

$$E_q = E_o \cos f(f(q,f)) \quad (12)$$

$$E_f = -E_o \cos q \sin f(f(q,f)) \quad (13)$$

$$f(q,f) = \frac{P_x}{E_o} AF(q,f) = \frac{\sin\left(\frac{bW}{2}\sin q \sin f\right)}{\frac{bW}{2}\sin q \sin f} \cos\left(\frac{bL}{2}\sin q \cos f\right) \qquad (14)$$

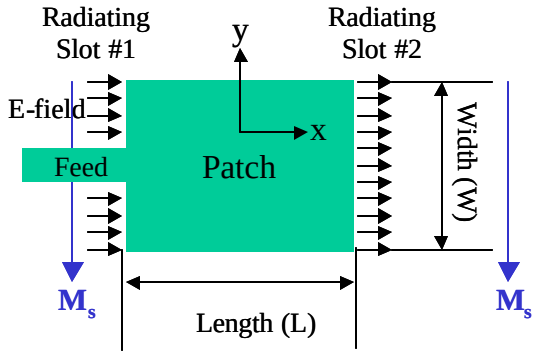

Figure 7. Top view showing the fringing electric fields that is responsible for radiation along with the equivalent magnetic surface (Ms) currents[23]

The cavity model provides a description of how the fields radiating from the surface of the patch antenna. Controlling the radiation characteristics of the patch with photonic crystals is the main principle in this thesis. Photonic crystals are explained in the following chapter.

[23] Stutzman and Thiele, *Antenna Theory and Design*, 2nd ed: John Wiley & Sons, Inc., 1998.

Chapter 3: Bandgap Substrates

In the past decade, a new technology has emerged which may be the key to developing ultra-wideband microstrip antennas. This technology manipulates the substrate in such a way that surface waves are completely forbidden from forming, resulting in improvements in antenna efficiency and bandwidth, while reducing sidelobes and electromagnetic interference levels. These substrates contain so-called Photonic Crystals.

3.1 History of Photonic Crystals

Photonic crystals are a class of periodic metallic, dielectric, or composite structures that exhibit a forbidden band, or bandgap, of frequencies in which waves incident at various directions destructively interfere and thus are unable to propagate[24,25]. Based on the dimensional periodicity of the crystal structure, the bandgaps can be in one, two, or three-dimensional planes, with the level of complexity increasing as the dimensions increase.

The first photonic-crystal structure conceptualized and manufactured was in 1991 by Eli Yablonovitch, then at Bell Communications Research in New Jersey. Yablonovitch fabricated the crystal structure by mechanically drilling holes a millimeter in diameter into a high dielectric constant material, as shown in Figure 8. This patterned material, which became known as “Yablonovite” prevented incident microwave signals from propagating in any direction along a unit sphere – in other words, it exhibited a 3-D

[24] Agi and Malloy, "Integration of a Microstrip Patch Antenna with a Two-Dimensional Photonic Crystal Substrate," *Electromagnetics*, vol. 19, 1999

[25] Parker and Charlton, "Photonic Crystals," *Physics World*, 2000

bandgap[26,27]. This structure has become the cornerstone for much of the research in this area with applications still in use today[28].

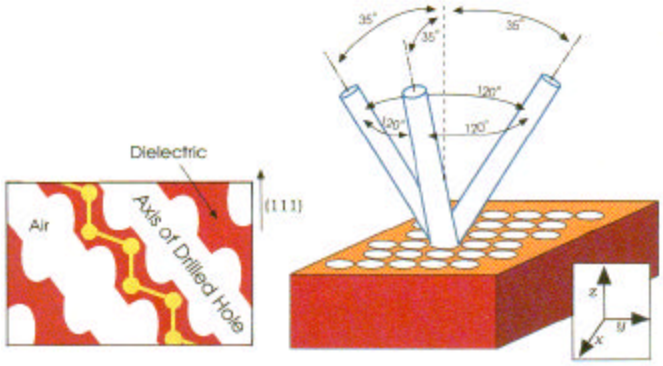

Figure 8. Technique used to fabricate the first 3D PC structure, the Yablonovite

In most communication applications, however, the use of Yablonovite is not practical. The three dimensional nature of the bandgap rejects incident energy from all directions around a unit sphere, making it better suited as a high efficiency reflector or mirror. Instead, in a 2-D photonic crystal, the bandgap exists only within a plane, thereby allowing propagation along one axis of the crystal. This is the ideal scenario for microstrip antenna designs, since the "rejection plane" could be in the plane of the patch to prevent surface wave formation. An example of a 2-D photonic crystal is a triangular lattice, shown in Figure 9. The details explaining this lattice structure and how a bandgap is formed will be discussed in the next section, along with some basic properties of crystals.

---

[26] Parker and Charlton, "Photonic Crystals," *Physics World*, 2000

[27] Agi and Malloy, "Integration of a Microstrip Patch Antenna with a Two-Dimensional Photonic Crystal Substrate," *Electromagnetics*, vol. 19, 1999

[28] Gonzalo and Martinez, "The Effect of Dielectric Permittivity on the Properties of Photonic Band Gap Devices," *Microwave and Optical Technology Letters*, vol. 23, 1999

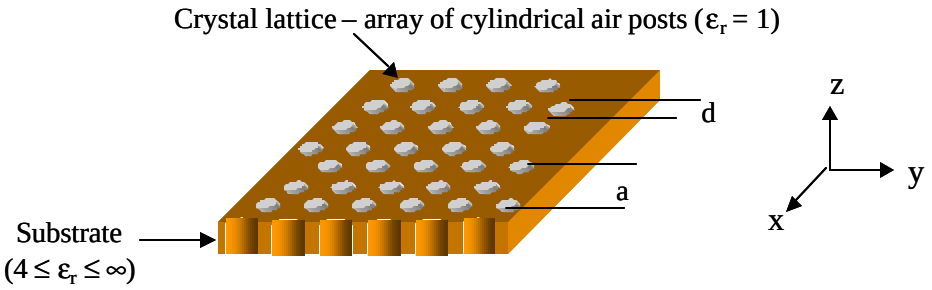

Figure 9. 2D photonic crystal structure patterned with a triangular crystal lattice; the crystal lattice is of cylindrical air posts in a high dielectric substrate

3.2 Basic Properties of Photonic Crystal

3.2.1 The Unit Cell

As stated in the American Heritage Dictionary of the English Language, a crystal is "a homogenous solid formed by a repeating, three-dimensional pattern of atoms, molecules, or shapes, having fixed distances between constituent parts". This replicating pattern is referred to as the unit cell of a crystal. Figure 10 illustrates the unit cell for the triangular crystal lattice shown in Figure 9. The unit cell contains all the pertinent information of the crystal such as the crystal geometry (shape, thickness, etc.), material properties (dielectric or magnetic), and the lattice spacing (shown as the dimension "a" in Figure 10) of each individual atom or molecule. It is this replicating unit cell that provides the periodicity in the crystal, and controls the location and extent of the bandgap.

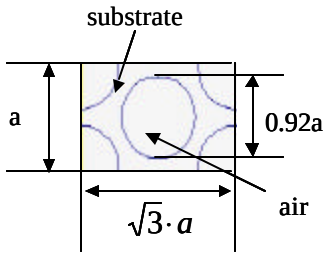

Figure 10. Top view of Figure 9, illustrating the unit cell of the triangular crystal lattice

3.2.2 The Bandgap

As a first order approximation, a bandgap is obtainable in a high dielectric material with integrated photonic crystals when an incident electromagnetic field propagates with a guide-wavelength (i.e. $l = \frac{c}{f\sqrt{e_r}}$) approximately equal to the lattice spacing of the crystal[29]. This rough approximation locates the center of the bandgap, which can extend higher than ±10% of the center frequency for high index materials[30]. A typical transmission coefficient (s_{12}) plot for a 2-port network, such as a microstrip transmission line, fabricated on a photonic crystal substrate is shown in Figure 11. This curve illustrates that as port 1 of the transmission line is excited, over 20dB of attenuation is experienced as the energy propagates from port 1 to port 2. Thus, the photonic crystal introduces a stopband filter response.

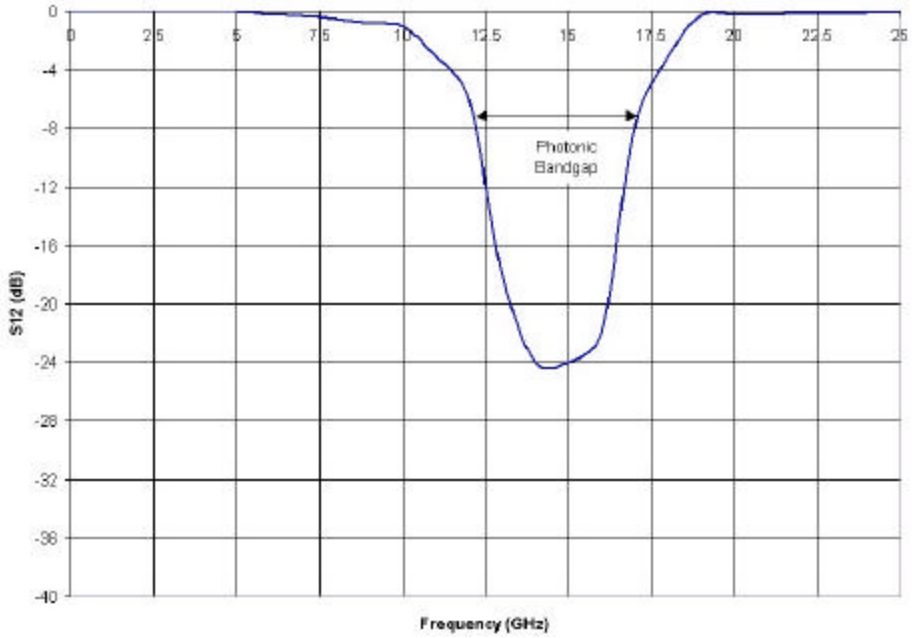

Figure 11. Transmission loss plot illustrating a bandgap in a microstrip transmission line at microwave frequencies

[29] Radisic and Qian, "Novel 2-D Photonic Bandgap Structure for Microstrip Lines," *IEEE Microwave and Guided Wave Letters*, vol. 8, 1998

[30] Parker and Charlton, "Photonic Crystals," *Physics World*, 2000

Indeed, the formation of the bandgap is dependent on the periodicity of the crystal, but it is also heavily dependent on the refractive index (dielectric constant) ratios between the base material (the substrate as a whole) and the impurities that form the crystal. Typically, the refractive index ratio must be at least 2:1 (substrate-to-impurity) ratio for the bandgap to exist[30]. For the 2-D triangular structure (Figure 9), the broadest bandgap is obtainable when the impurities (the cylindrical post) are of air (ε_r =1), while the base material is a high dielectric constant (for example, ε_r =10). A 10:1 dielectric (3.16:1 refractive index) ratio would satisfy the index requirement and form a broad bandgap, with proper crystal spacings. This explains the need for a high dielectric substrate for a patch antennas designed on a photonic crystal substrate.

3.2.3 Defects in Periodicity

A photonic crystal essential behaves much like a bandstop filter, rejecting the propagation of energy over a fixed band of frequencies. However, once a defect is introduced such that it disrupts the periodicity in the crystal, an area to localize or "trap" electromagnetic energy is established. In this region, a passband response is created. This ability to confine and guide electromagnetic energy has several practical applications at microwave frequencies as filters, couplers, and especially antennas.

This rather simple concept of placing defects in a photonic crystal structure introduces a new methodology in the design of microstrip (patch) antennas. The idea is to design a patch antenna on a 2D photonic crystal substrate, where the patch becomes the "defect" in the crystal structure, as shown in Figure 12. In this case, a crystal array of cylindrical air holes are patterned into the dielectric substrate of the patch antenna. By not patterning the area under the patch, a defect is established in the photonic crystal, localizing the EM fields. Surface waves along the XY plane of the patch (Figure 12) are forbidden from forming due to the periodicity of the photonic crystal in that plane. This prevention of surface waves improves operational bandwidth and directivity, all

while reducing sidelobes and coupling, which are common concerns in microstrip antenna designs.

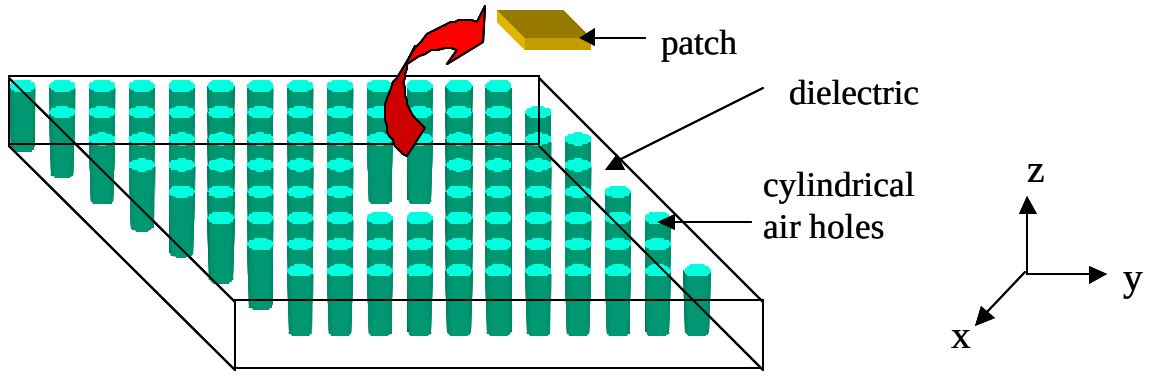

Figure 12. Illustration of a patch designed on a photonic crystal substrate; defect introduced in the area under the patch

Using these concepts, a photonic crystal patch antenna was developed. The following section describes the analytical analysis of photonic crystals and how to integrate photonic crystals with microstrip antennas.

Chapter 4: Electromagnetic Field Analysis of PBG

There is extensive ongoing research in developing theoretical methods to help evaluate the dispersion relations in multidimensional photonic crystals. Typically, these models require complex analytical programs to compute the absorption, reflection, and transmission coefficients of the photonic crystal structure as it is illuminated at different angles of incidence around a unit sphere. In general, it is difficult to get an intuitive grasp of the solutions to Maxwell's equations at different special points in complex dielectric structures[31]. Due to the complexity of some lattice structures, oftentimes a new model is required for each variation in periodicity, geometry, thickness, etc. Therefore, for simplicity this chapter will only discuss some of the basic electromagnetic properties of the specific 2D triangular photonic crystal structure. The structure contains periodic cylindrical air posts in a high dielectric substrate, as required for the design of patch antennas. This discussion will begin with identifying the so-called Brillouin Zone.

4.1 Brillouin Zone

The study of waves in periodic structures makes use of a single physical principle proposed by Floquet in 1884. Floquet's principle states that normal modes in periodic structures can be expressed as a superposition of a set of plane waves whose wave vectors are related by

$$\vec{k}_n = \vec{k}_o + n\vec{G} \qquad (15)$$

where $\vec{k}_o$ is the initial arbitrary wave vector, $\vec{k}_n$ is the wave vector of the nth mode, and $\vec{G}$ is the reciprocal lattice vector. Reciprocal lattice vectors mathematically represent

[31] Meade, Rappe, Brommer and Joannopoulos, "Nature of the photonic bandgap: some insights from field analysis," *J Opt Soc Am B*, vol. 10, pp. 328-332, 1993

the crystal's unit cell by describing how the repeating units tile together without establishing overlapping regions. These vectors are defined in the $\vec{k}$ space and expressed as

$$\vec{b}_1 = 2p\,\frac{\vec{a}_2 \times \vec{a}_3}{\vec{a}_1 \cdot (\vec{a}_2 \times \vec{a}_3)} \tag{16}$$

$$\vec{b}_2 = 2p\,\frac{\vec{a}_3 \times \vec{a}_1}{\vec{a}_1 \cdot (\vec{a}_2 \times \vec{a}_3)} \tag{17}$$

$$\vec{b}_3 = 2p\,\frac{\vec{a}_1 \times \vec{a}_2}{\vec{a}_1 \cdot (\vec{a}_2 \times \vec{a}_3)}, \tag{18}$$

where the vectors $\vec{a}_1, \vec{a}_2$, and $\vec{a}_3$ are obtained from the unit cell as shown in Figure 13.

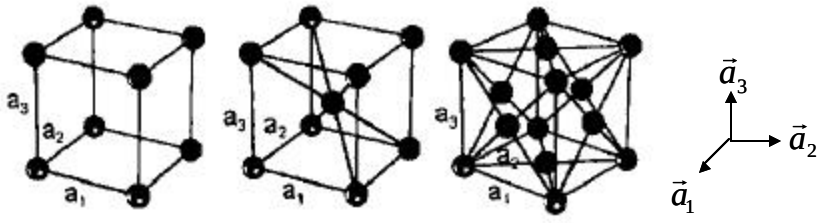

Figure 13. Lattice vectors for different cubic structures. (a) Simple cubic, (b) Body centered cubic, (c) Face centered cubic[32]

Later Bloch extended Floquet's theorem such that it covers multidimensional periodic structures as well. This extension is referred to as the Bloch expansion theorem. Bloch's theorem computes the modes of an electromagnetic wave propagating through a periodic structure by using

$$H_k(r) = e^{jkr}\,u_k(r) = e^{jkr}\,u_k(r+R) \tag{19}$$

[32] Gonzalo, "Enhanced Patch-Antenna Performance by Suppressing Surface Waves Using Photonic-Bandgap Substrates," *IEEE Transaction on Microwave Theory and Techniques*, vol. 47, 1999

The significance of this theorem is that different values of "k" do not necessarily lead to different propagating modes. Specifically, a mode with wave vector $\vec{k}$ and a mode with wave vector $\left(\vec{k}+\vec{G}\right)$ are the same mode if $\vec{G}$ is a reciprocal lattice vector[32].

Consequently, there is redundancy in the label *k*, which allow calculations to be simplified to cover a finite zone in the reciprocal space oppose to the entire crystal structure. In other words, values of *k* that lie outside of this zone can be reached from within the zone by adding $\vec{G}$ and are, therefore, redundant labels. This zone is defined as the Brillouin zone.

In general, crystal structures are definable via an infinite number of Brillouin zones. However, for the analysis of photonic crystals, we are mainly interested in the so-called first Brillouin zone. Identification of the first Brillouin zone is accomplished through a straightforward approach, as pictorially explained in Figure 14.

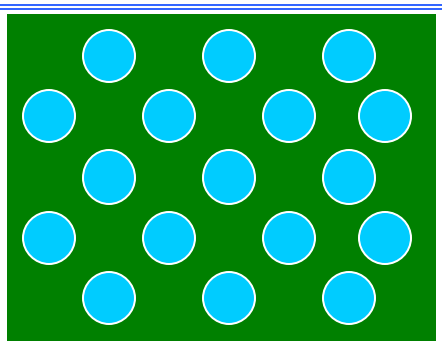

(a) Starting at origin, draw lines to the nearest lattice points

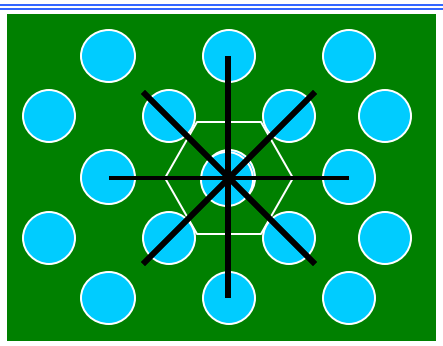

(b) Connect points bisecting axes to form 1st Brillouin zone.

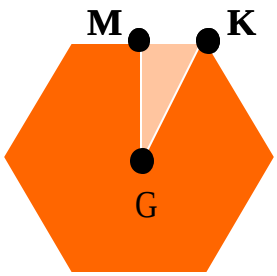

(c) The 1st Brillouin zone and symmetry points of the triangular lattice.

Figure 14. Graphical method used to determine the 1st Brillouin Zone of a crystal lattice structure

The smallest region within the Brillouin zone for which the k directions are not related by symmetry is called the irreducible Brillouin zone[33]. This irreducible zone for a triangular pattern is itself a triangle as illustrated in the tapered-line section in Figure 14(c). The rest of the Brillouin zone, colored in orange are redundant copies of the irreducible zone and are unnecessary for calculations of the bandgap.

4.2 Electromagnetic Fields in Photonic Crystals

The propagation of electromagnetic energy is governed by the four Maxwell equations, namely

$$\nabla \cdot \vec{H}(r,w) = 0 \tag{20}$$

$$\nabla \cdot \vec{e}(r,w) \cdot \vec{E}(r,w) = 0 \tag{21}$$

$$\nabla \times \vec{E}(r,w) = -jw\vec{B} \tag{22}$$

$$\nabla \times \vec{H}(r,w) = -jw\vec{e}(r,w) \cdot \vec{E}(r,w) \tag{23}$$

These standard equations depend on both frequency and spatial position requiring the use of complex numerical codes to formulate the equation system for eigenvalues and eigenvectors in a PC[34]. The calculation required to solve such equations is beyond the scope of this thesis. Instead, software specifically designed for the analysis of photonic crystals will be used to calculate the bandgap of the triangular lattice crystal. This software is discussed in ***Chapter 5***.

[33] Meade, Rappe, Brommer and Joannopoulos, "Nature of the photonic bandgap: some insights from field analysis," *J Opt Soc Am B*, vol. 10, pp. 328-332, 1993

[34] Gonzalo, "Enhanced Patch-Antenna Performance by Suppressing Surface Waves Using Photonic-Bandgap Substrates," *IEEE Transaction on Microwave Theory and Techniques*, vol. 47, 1999

4.3 Antennas Using Photonic Crystal Substrates

With the ability to completely prohibit the propagation of electromagnetic energy at specific frequencies, photonic crystals and their respective bandgaps correlate well with the development of next-generation microstrip antennas. The insertion of photonic crystals into the substrate does not change any of the fundamental trade-offs that exist for patch antennas. In other words, the antenna designer must still chose between using a thick or thin substrate. The only requirement is that the refractive index ratio between the substrate and crystals be large enough (greater than 2:1) for the bandgap to exist. This section compares two methodologies of introducing photonic crystals into patch antenna designs. Namely, thick and thin substrate approaches. This section concludes with a novel technique, which combines properties of both approaches when using the photonic crystal structure shown in Figure 12.

4.3.1 Thick Substrates

The concept of designing microstrip antennas on a thick photonic crystal substrate is to utilize quasi-3D bandgaps to radiate electromagnetic field from the antenna, without using a ground plane. The ground plane is removable because the 3D bandgap creates an equivalent ground plane due to total internal reflections caused by the high index ratios in the vertical axis (perpendicular to the patch), as shown in Figure 15.

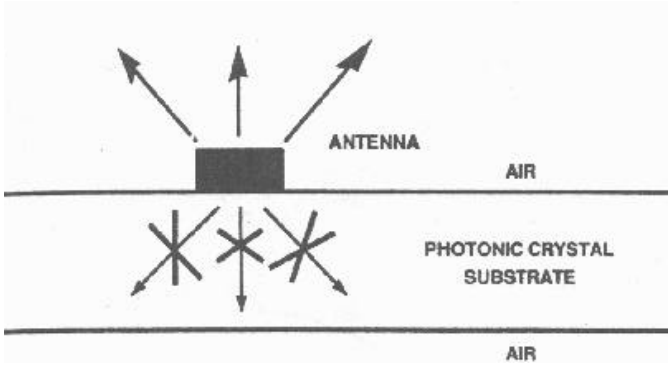

Figure 15. Cross-sectional view of a Patch Antenna radiating from a Thick PBG

In research performed by Brown et al.[35], a thick substrate patch antenna was fabricated using a triangular photonic crystal, which is consistent with the structure in Figure 12. These crystals are periodic in two dimensions, namely in the XY plane in Figure 12, forming a 2D bandgap. The third dimension of periodicity is a result of total internal reflection - at specific angles of incidence (greater than the critical angle), electromagnetic waves that transverse through a high permittivity material (substrate) into to a lower permittivity material (air) would, ideally, perfectly reflect and become contained within the higher permittivity material. This is defined as a "quasi-3D bandgap" since energy is allowed to propagate at angles less than the critical angle. With this third dimension in the bandgap, the ground plane can be removed.

In a comparison study, Brown measured dramatic improvements in surface wave reduction when photonic crystals were inserted into the substrate of a conventional microstrip antenna. In his journal article[36], he also reported a decrease in back radiation with a front-to-back pattern ratio of 24 dB, opposed to 12 dB for the conventional patch antenna.

Despite the significant improvements identified in Brown's study, this style of antenna is not very practical. First, the substrate thicknesses required for these antennas are cited over eight centimeters for a frequency of 13.2 GHz. At such high frequencies, this substrate is too large for most standards, making the substrate an appreciable size in comparison to the patch. Second, the lack of a ground plane causes many grounding complications when feeding the antenna. The direct-coupled microstrip feed is eliminated since microstrips require a ground plane for operation. Therefore, the

[35] Brown and Parker, "Radiation Properties of a Planar Antenna on a Photonic-Crystal Substrate," *J Opt Soc Am B*, vol. 10, 1993

[36] Brown and Parker, "Radiation Properties of a Planar Antenna on a Photonic-Crystal Substrate," *J Opt Soc Am B*, vol. 10, 1993

antenna is limited to only the coaxial probe and the proximity coupled feeds. To resolve these issues, antennas designed on thin substrates incorporating photonic crystals have also been investigated.

4.3.2 Thin Substrates

The concept of using thin substrates containing photonic crystals to design microwave devices was first conceived by Radisic et al. in 1998[37]. In their approach, microstrip filters were fabricated by simply etching a two-dimensional triangular pattern into the ground plane of a conventional microstrip line. This resulted in nearly 100% reflection loss over a span of frequencies governed by the lattice spacing, opposed to the typical 100% transmission expected from a microstrip line. Coccioli et al. later expanded Radisic's concepts to incorporated this approach in the development of microstrip antennas printed on thin substrates containing similar photonic crystals[38]. Figure 16 illustrates a facsimile of the antenna constructed in their study. Experimental measurements of this type of antenna illustrated a 10dB sidelobe level reduction and minimal reduction in front-to-back ratios[38] when compared to a patch without the photonic crystals.

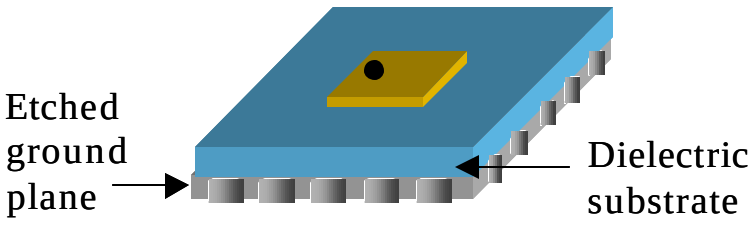

Figure 16. Photonic crystals etched in the ground plane of a patch designed on a thin substrate

[37] Radisic and Qian, "Novel 2-D Photonic Bandgap Structure for Microstrip Lines," *IEEE Microwave and Guided Wave Letters*, vol. 8, 1998

[38] Coccioli, Deal and Itoh, "Radiation Characteristics of a Patch Antenna on a Thin PBG Substrate," *IEEE Transaction on Antennas and Propagation*, vol. 45, pp. 656-659, 1998

Later in 1999, Agi et al. proposed another version of a microstrip antenna with photonic crystals integrated in a thin substrate. In their approach, the holes for the triangular crystal were etched into the substrate[39], leaving the ground plane unmodified. This is similar to the thick substrate approach (Carbonell) discussed above, but in this case, the ground plane is included. Their research illustrated a slight increase in the resonance bandwidth of the antenna, a 4.5 dB increase in the depth of the resonance point, and radiation pattern front-to-back ratio improvements as high as 5 dB[39].

These thin substrate designs exhibit comparable results to that of the thick substrate designs. The only drawback, however, is that the bandgap is reduced to two dimensions, due to the inclusion of the ground plane – total internal reflections condition scarified. To reestablish the third dimension of the bandgap, a new approach is required.

4.3.3 Three-dimensional Bandgaps using Thin Substrates

In order to reestablish the third dimension of the bandgap, a technique typically reserved to tune the resonant frequency of a patch was used. Dahrele et al. first introduced this technique in the early 1980's[40]. Their relatively simple concept is to introduce airgaps between the dielectric and the ground plane to induce changes in the effective permittivity of the dielectric substrate. This multilayer stacking of dielectrics causes the resonant frequency ($l_r = \frac{c}{f_r \sqrt{e_{eff}}}$) of the patch to shift by lowering the effective permittivity (e_{eff}) by increasing the airgap spacing. As a result, the resonant

[39] Agi and Malloy, "Integration of a Microstrip Patch Antenna with a Two-Dimensional Photonic Crystal Substrate," *Electromagnetics*, vol. 19, 1999

[40] Dahrele and Lee, "Theory and experiment on microstrip antennas with air gaps," *IEE Proceeding Microwave and Antenna Propagation*, vol. 132, 1985

frequency of the patch becomes tunable without requiring adjustments to the dimensions of the patch, as typically required in practice.

This design strategy not only provides a way to tune a patch antenna, but also establishes a technique to introduce a 3D bandgap in a thin substrate patch design. Using this technique, along with Agi's approach[41], the 3D bandgap consists of two dimensions of periodicity of the photonic crystals in the plane of the patch and a third dimension from total internal reflection rules, as in the thick substrate case. This novel approach is illustrated in Figure 17. The design and fabrication of this type of patch antenna is discussed in Chapter 6.

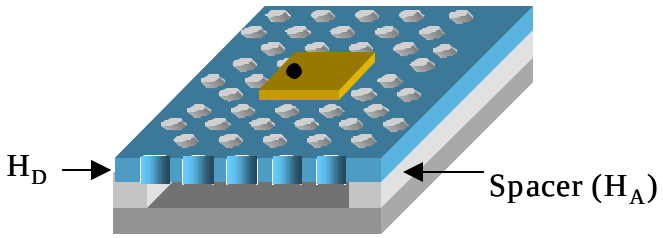

Figure 17. Design of novel patch antenna designed on a thin substrate with photonic crystals. H_D is the height of the dielectric and H_A is the thickness of the airgap

[41] Agi and Malloy, "Integration of a Microstrip Patch Antenna with a Two-Dimensional Photonic Crystal Substrate," *Electromagnetics*, vol. 19, 1999

Chapter 5: Analytical Design Software

Commercial simulator software was utilized in the development of models for the patch antennas and photonic crystals. This chapter serves as an introduction of these packages.

5.1 Antenna Design Software

To analytical evaluate the patch designs, the High Frequency Software Simulator (HFSS©), developed by Agilent Technologies, was utilized. HFSS is an interactive software package that computes s-parameters and full-wave field solutions for arbitrarily shaped 3D passive structures. An adaptive meshing technique is used to define regions where finite element method (FEM) calculations analytically evaluate the structure. The accuracy and flexibility of the software package is its main advantage.

One of the key functions of this software is its ability to specify the constitutive parameters of the substrate and the surrounding medium. As illustrated in Figure 18, the user is capable of entering the relative permittivity and permeability and the corresponding loss tangents. Although not shown, complex materials are also plausible. The solutions extracted from HFSS will be the foundations to predict performance and tolerance of the antenna design in this project. Details for drawing the antenna in HFSS will be discussed, as necessary, in subsequent sections.

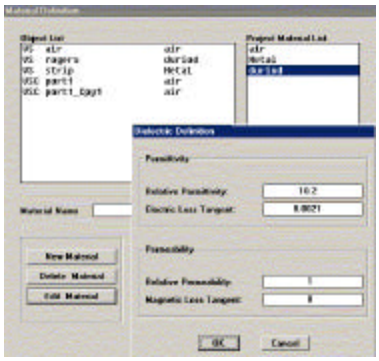

Figure 18. Material Definitions Screen in HFSS

5.2 Bandgap Analysis Software

Numerical evaluation of the location and extent of the bandgap is performed using software called Translight©, a shareware graphic-user interface (GUI) distributed through the Department of Electronics & Electrical Engineering at the University of Glasgow. The code uses user definable "building blocks" or the unit cells, which are cascade in any direction to form photonic crystals. The software computes the reflection and transmission coefficients as electromagnetic signals are applied, at multiple angles of incidence, to the photonic crystal. At each incidence angle, the coefficients are measured over a span of frequencies. The results are tabulated and then plotted to identify the bandgaps. An image of the main menu screen is illustrated in Figure 19.

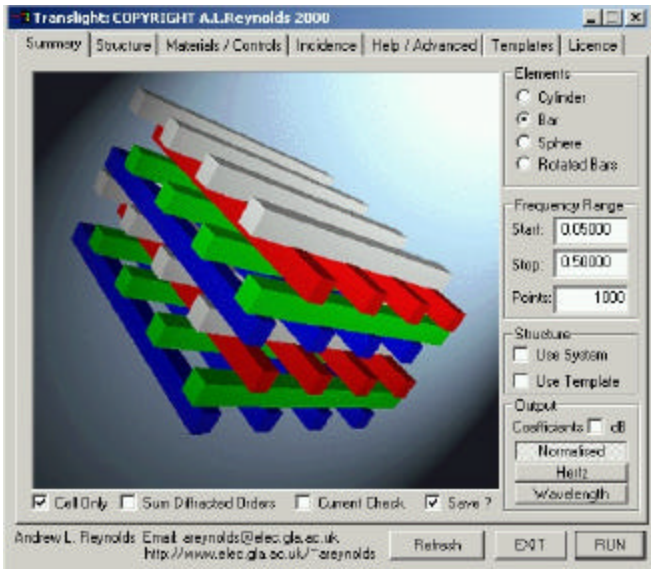

Figure 19. Main menu screen for the Translight software used to estimate the extent and location of the bandgap

These two software packages were implemented in the design and analysis of the microstrip antennas and the photonic crystals. The following chapter details the design of the antennas and the simulated results obtained from the separate softwares.

Chapter 6: Design of Patch Antenna

In order to identify the improvements in this novel photonic crystal based patch antenna, designed on a thin substrate with an airgap as compared to the previous thin substrate designs, some common characteristics must be identified. The three parameters held constant throughout the study are the shape of the patch (square), the frequency of operation (9.5 GHz), and the dimensions and material properties (lattice spacing and index ratio) of the photonic crystals. The results of the thick substrate antennas were not included in this comparison because measurements on that antenna were at 13.2 GHz. The following procedures explain the analysis techniques required to design these antennas.

6.1 Frequency Selection and Airgap Thickness

The first step in designing the patch antenna was to select the frequency of operation. Since the goal of this thesis was to illustrate improvements over the thin substrate photonic crystal patch designed by Agi et al.[42], **it was decided to design the patch to resonate at 9.5 GHz,** which is the frequency Agi used. However, due to the airgap separating the ground plane and dielectric substrate, this was not a trivial step as will be explained.

To evaluate the effects of the airgap, an equivalent permittivity (ε_{re}) was calculated to substitute for the relative permittivity (ε_r) – the dielectric constant for the substrate alone. This is a common procedure for designing microstrip transmission lines, where the dielectric constant of the substrate is combined with that of the outside

[42] Agi and Malloy, "Integration of a Microstrip Patch Antenna with a Two-Dimensional Photonic Crystal Substrate," *Electromagnetics*, vol. 19, 1999

environment[43]. For the airgap dielectric substrate, the equivalent permittivity can be evaluated using the equation[44]

$$e_{re} = \frac{e_r (H_D + H_A)}{(H_D + H_A e_r)}, \qquad (24)$$

where H_D is the dielectric thickness, H_A is the airgap thickness, and ε_r is the relative permittivity.

Based on this expression, it can be shown mathematically that as H_A increases, ε_{re} decreases. Therefore, the resonant frequency (f_r) will increase ($f_r = \frac{c}{l\sqrt{e_{re}}}$, where c is the speed of light and λ is fixed) with increased airgap height. Empirical results from [44] illustrating this point are tabulated in Table 1. However, it should be noted that resonance does not increase linearly with H_A. As observed in the fourth row of data, the resonant frequency without an airgap (H_A = 0) is 5.96 GHz. A 0.5 mm airgap tunes resonance up to 6.05 GHz, however, when H_A = 1.0 mm the resonance starts to descend to 6.01 GHz. This phenomenon is also illustrated in the fifth row of data between H_A = 0.5 mm and H_A = 1.0 mm. Therefore, to avoid this region of non-linearity, it was decided to design the patch antenna using **an airgap height of H_A = 0.25 mm.**

[43] Pozar, *Microwave Engineering*, 2nd ed: John Wiley & Sons, Inc., 1998.
[44] Abboud, Damiano and Papiernik, "Accurate Model for the input impedance of coax-fed rectangular microstrip antenna with and without airgaps," *Proceedings of the IEEE*, vol. 135

			Resonant Frequency in GHZ		
W (cm)	**L (cm)**	**H_D (cm)**	**H_A = 0 mm**	**H_A = 0.5 mm**	**H_A=1.0mm**
5.70	3.80	0.3175	2.38	2.51	2.57
4.55	3.05	0.3175	2.91	3.05	3.10
2.95	1.95	0.3175	4.29	4.42	4.45
1.95	1.30	0.3175	5.96	6.05	6.01
1.70	1.10	0.3175	6.76	6.81	6.73

Table 1. Measured HP-8510 results for rectangular patches designed with various airgap thicknesses[45]

In the linear region, the resonant frequency increases with increased airgap height. To account for this increase, the patch had to be designed at a lower than desired frequency. This will be discussed in Section 6.3.

6.2 Substrate Material Selection

The second step in the design procedure was to specify a substrate material, which is governed by the photonic crystal requiring a high permittivity ratio between the substrate and crystal. A common thin substrate with a high dielectric constant is the Rogers Corporation material RT/Duriod 6010.2. The manufacturer specs for the RT/Duriod 6010.2 are as follows.

Dielectric Constant: $\varepsilon_r = 10.2 \pm 0.25$ (25)

Dissipation Factor @ 10 GHz: $\tan \delta = 0.0023$ (26)

Substrate Height (H_D) = 50 mils (1.27 mm) (27)

[45] Abboud, Damiano and Papiernik, "Accurate Model for the input impedance of coax-fed rectangular microstrip antenna with and without airgaps," *Proceedings of the IEEE*, vol. 135

It should be noted that the material issued by the manufacturer as "samples" and could have contained inherent defects.

For the remainder of the paper, the RT/Duriod 6010.2 material will be referred to as the substrate. These specs for the substrate are used for all proceeding calculations and simulations.

6.3 Design of Patch

6.3.1 First Order Approximations

To comply with Agi's design[46], the antenna was configured as a square patch. This simplifies the design since the dimensions are on the order of a half-wavelength, as evaluated in equation (28). With the values for the dielectric constant (ε_r), resonant frequency (f_r = 9.5GHz), and substrate height (H_D) already specified, these calculations are quite trivial. However, as stated before, the airgap induces an increase in the resonant frequency of the patch. Thus, to compensate for the shift, instead of calculating the dimensions at 9.5 GHz, equation (28) was evaluated using a resonant frequency of 9.0 GHz. The result of this calculation is shown in equation (29).

$$\text{Length or Width: } L = W = \frac{c}{2 f_r \sqrt{m_r e_r}} = \frac{l_g}{2} \qquad (28)$$

$$W = L = 5.2 \text{ mm (at 9.0 GHz)} \qquad (29)$$

With the patch dimension selected, the final step in the design was to verify patch resonance and locate the proper placement of the probe. HFSS was utilized to accomplish this final step.

---

[46] Agi and Malloy, "Integration of a Microstrip Patch Antenna with a Two-Dimensional Photonic Crystal Substrate," *Electromagnetics*, vol. 19, 1999

6.3.2 Verification using HFSS

Utilizing the airgap height, parameters of the substrate, and dimensions of the patch, a 3-D HFSS model was created to locate the optimum location of the feed and predict the performance of the antenna. The HFSS model developed for this analysis is shown in Figure 20. The goal was to achieve the resonance with optimum characteristics, which was accomplished using a trial-and-error approach to locate the probe excitation point. HFSS calculates the scattering parameters of multi-port matrixes by exciting each port separately and measuring the frequency response through the other non-excited ports with respect to excited port. In the case of a patch antenna, the device is a single port device, therefore, only the return loss (S_{11}) parameter is measured, which is a measurement of the match between the antenna and the feed. From this measurement, the resonant frequency of the patch can be located by observing the location of the deepest null - the best match between patch and feed.

For the airgap patch design, the location of the feed that provided the correct resonant frequency and highest "match" is shown in Figure 21. The corresponding simulated results are illustrated in Figure 22.

The results in Figure 21 illustrate some important properties of the patch antenna designed with an airgap. First, despite using the dimensions for a conventional square patch design to resonates at 9.0 GHz, i.e. L=W= 5.2 mm, the simulation illustrates resonance at 9.5 GHz. Therefore, the airgap is, indeed, lowering the effective dielectric constant and increasing the resonant frequency of the patch. Second, the 10dB operational bandwidth is 500 MHz or 5.26% (f_r / 10dB BW). Conventional patch designs, without airgaps, typically only resonant with less than 3.0% bandwidth. It is believed that the addition of the photonic crystals will further improve these characteristics.

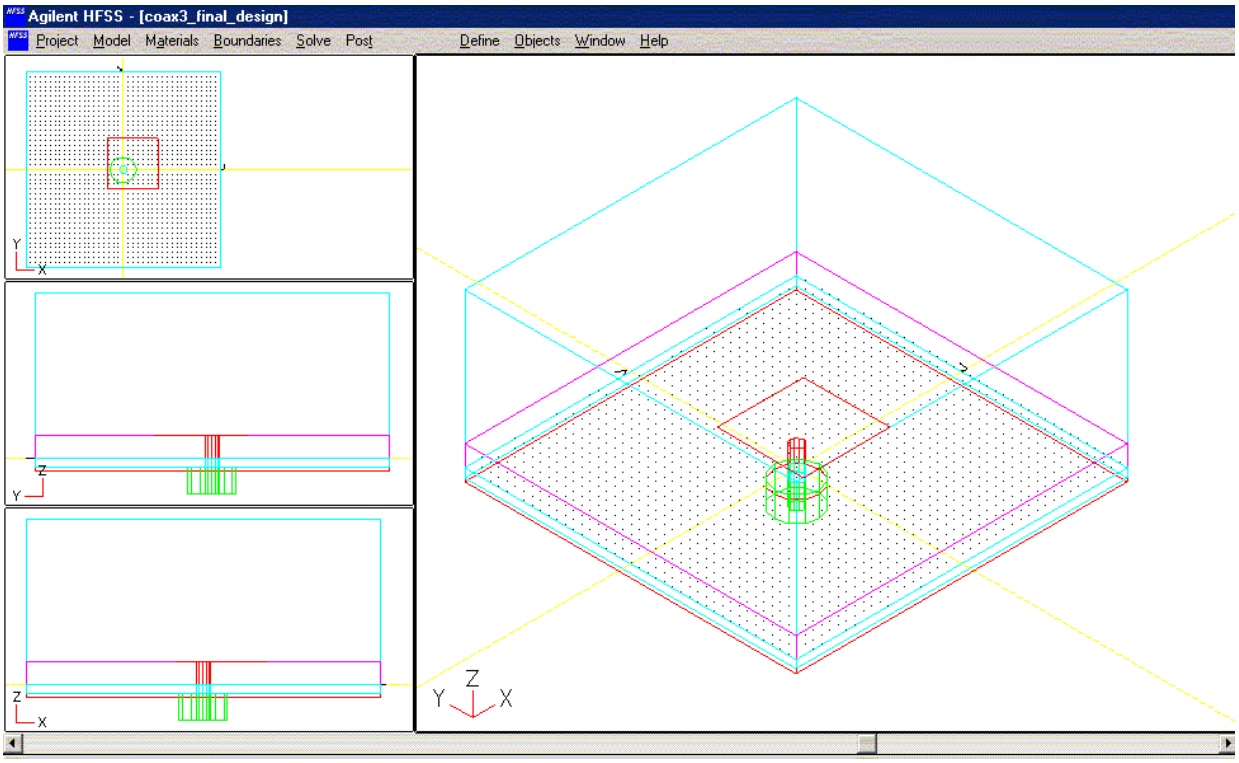

Figure 20. HFSS simulation model used to evaluate a patch antenna with an airgap

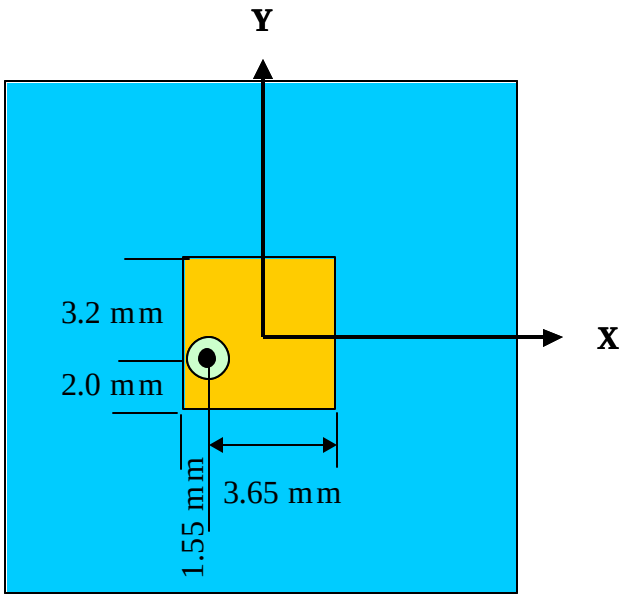

Figure 21. Final dimensions for the patch; placement of probe feed. The coordinate system matches the coordinate system used in the model (Figure 12)

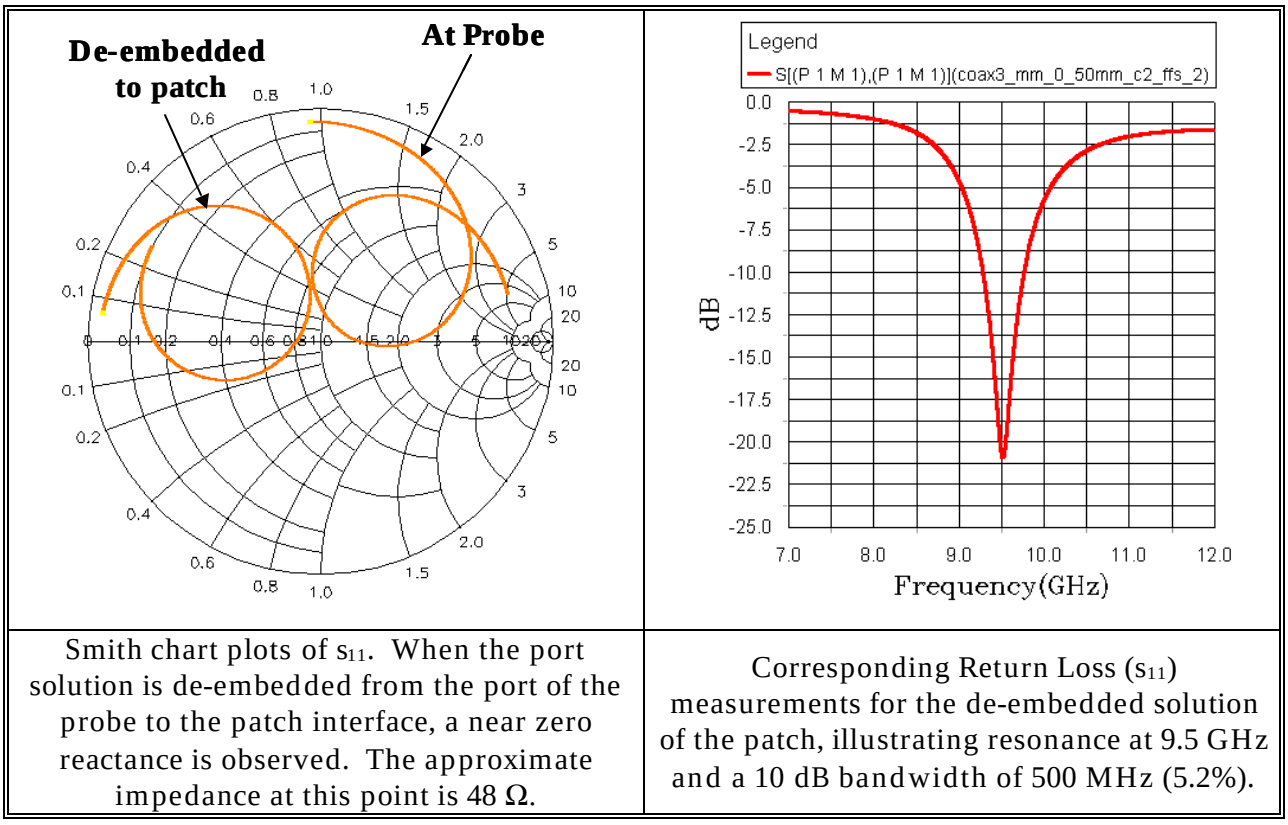

Smith chart plots of s_{11}. When the port solution is de-embedded from the port of the probe to the patch interface, a near zero reactance is observed. The approximate impedance at this point is 48 Ω.

Corresponding Return Loss (s_{11}) measurements for the de-embedded solution of the patch, illustrating resonance at 9.5 GHz and a 10 dB bandwidth of 500 MHz (5.2%).

Figure 22. Corresponding HFSS results for the patch antenna described in Figure 21

6.3.3 Explanation of HFSS Model

Since the HFSS software may be new to the reader, it is appropriate to explain the model in some detail. As illustrated in Figure 20, the HFSS drawing window is divided into four different perspectives. The view to concentrate on is the large-3D view on the right. There are six shapes in this view excluding the drawing grid, which is irrelevant in this explanation. Starting with the lowest rectangular structure, with respect to the z-axis, the first layer, shown in red, depicts the ground plane for the antenna. Proceeding along the z-axis, the next layer is the airgap, colored in blue, separating the dielectric and the ground plane. The next geometry is substrate purple in color. The next blue rectangular box is a large radiation boundary for the antenna. The radiation boundaries prevent HFSS from applying metal over this region, thus allowing the patch to radiate into free space. To ensure calculations are in the far field, the radiation boundary must

be several wavelengths in extent. The patch is the thin red square located between the air boundary and the dielectric. The remaining two cylindrical objects model the coaxial probe, consisting of a center conductor (red) and an outer conductor (green).

The center conductor for the coaxial probe travels through the airgap and dielectric substrate and physically connects to the patch antenna. It is modeled as a perfectly conducting metal as is the patch. The outer conductor of the probe stops at the ground plane-airgap interface. It is modeled as a cylinder with Teflon ($\varepsilon_r = 2.2$) as the dielectric constant, as specified by Digi-Key Part #: J493-ND. The dielectric properties of each geometry in the model are specified in a window similar to Figure 18.

This explains the HFSS model for the patch antenna designed with an airgap between the substrate and ground plane. Attempts to model the antenna incorporating photonic crystals in the substrate proved unsuccessful due to the number of objects in the model. Despite this minor setback, separate software was utilized to determine the location and extent of the bandgap, as explained in the next subsection.

6.4 Comments on Designing a Patch on a Photonic Crystal Substrate

The bandgap associated with a specific triangular crystal structure is completely independent of the design of the antenna. Therefore, when designing a patch antenna on a substrate containing photonic crystals, the dimensions of the antenna, i.e. width, length, or substrate thickness, remain constant. This is possible since the area under the patch is unperturbed, except for the insertion of the probe.

As previously stated, the patch antennas were designed using photonic crystals with a unit cell consisting of cylindrical posts as shown in Figure 10. To comply with Agi's design[47], the parameters of the unit cell were selected as:

Lattice Constant: a = 1.38 cm, and (30)

Post Diameter: d = 1.27 cm. (31)

These dimensions establish a bandgap centered at 9.0 GHz[48]. This was verified using the photonic crystal software, discussed above in Section 5.2, as graphically illustrated in Figure 23. The graph displays a bandgap located at 9.2 GHz with a 3dB bandwidth (from the max) of approximately 1.7 GHz. It should be noted that the data curves represent the reflectivity response as the photonic crystal structure is illuminated in one direction of radiation, along the XZ plane in Figure 12. Similar reflectivity curves were observed as the structure was illuminated over 360 degrees in the XY plane, verifying the existence of a two-dimensional bandgap. These results agreed with Agi's result[48].

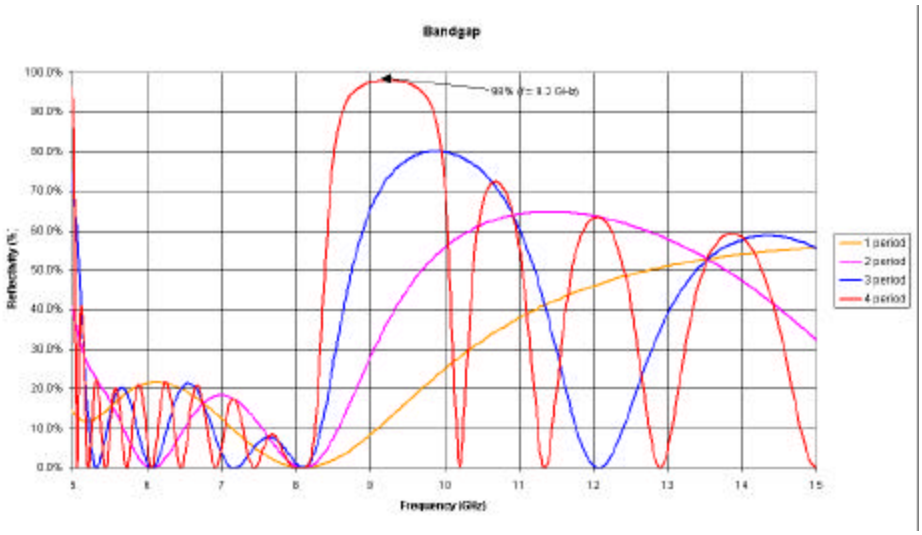

Figure 23. Translight simulation identifying the extent and location of the bandgap for the crystal geometry described in Agi's paper

[47] Agi and Malloy, "Integration of a Microstrip Patch Antenna with a Two-Dimensional Photonic Crystal Substrate," *Electromagnetics*, vol. 19, 1999

[48] Agi and Malloy, "Integration of a Microstrip Patch Antenna with a Two-Dimensional Photonic Crystal Substrate," *Electromagnetics*, vol. 19, 1999

An extremely important observation in the Translight results is how the bandgap shifts as the number of periods increase. As observed in the Figure 23, to obtain a reflectivity response as high as 98.0% (i.e. 34dB of attenuation) the crystal structure must extend for four periods. This information sets fabrication boundary conditions that must be satisfied to achieve the proper bandgap response.

Chapter 7: Fabrication Process

This section describes the manufacturing processes required to design microstrip (patch) antennas, printed on a substrate with and without photonic crystals, and with an airgap separating the ground plane and substrate. The issue of tolerance is also addressed in this section, which provides some insight into problems related to measurement that will be discussed in the next chapter.

7.1 Without Photonic Crystal in the Substrate

Initially, a baseline patch antenna was fabricated with only a 0.25 mm airgap and no photonic crystal in the substrate. An LPKF® Laser and Electronics Printed Circuit Board (PCB) milling station, illustrated in Figure 24, was employed for the fabrication. Essentially, the milling station selectively mills away copper from a dielectric substrate, leaving behind a pattern in the form of the square patch. It was also used to accurately place a small hole through the substrate, which, for the purpose of patch antennas, establishes an entry point for the center conductor of the coaxial probe to connect to and feed the patch antenna. This hole was formed with a specialized drill bit with roughly the diameter of the center conductor of an SMA connector. The author would like to acknowledge Chris Anderson from MPRG whom fabricated the patches used in this research.

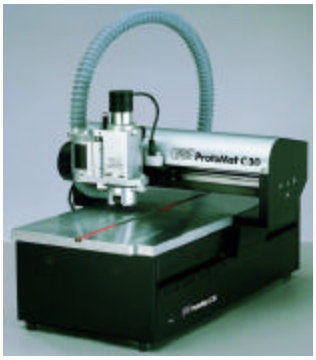

Figure 24. LPKF milling station used to fabricate patch antennas

Unfortunately, at X-band frequencies, this system is limited by manufacturing tolerances. First, the LPKF milling station operates using specialized milling and drill bits specific to their station. Therefore, over time and with continued use, the drill bits become dull and lose the tolerance specified by the manufacturer. For example, the cutting width of the milling bit controls how much copper is removed as the drill passes over the substrate. Therefore, without high quality bits, there is a substantial probability for error. In addition, due to the circular nature of the milling bit, there are also concerns about rounded edges. Thus, perfect squares are not easily obtainable. These fabrication tolerances are important, especially at higher frequencies, because a slight error could result in major degradations in antenna performance.

Continuing with fabrication process, once the square patch is etched onto the surface of the substrate, the remaining copper, on the same side of the patch, is removed. This step is performed by physically pulling the copper off the substrate with razor blades and a pair of tweezers. Since the substrate comes with a double cladding of cooper, all the copper on the opposite side had to be removed as well. This establishes the airgap to separate the substrate from the ground plane.

A second piece of copper-cladded substrate establishes the ground plane for the antenna. This piece was cut with roughly the same dimensions as the substrate containing the patch. Teflon screws hold the two substrates together along the six edges of the substrate. Seastrom Manufacturing Teflon washers with a thickness of ½mm maintain the separation between the two substrates, forming the airgap. It is important to note that other side of the second piece of substrate, not be used as the ground plane, had to be removed prior to testing. This reduces the risk of any false resonance that may appear while the antenna is being measured.

Before attaching the substrates, the probe had to be connected to the patch. This was accomplished using a 50 Ω 4-Hole Flange SMA coaxial connector, manufactured by

Johnson. As mentioned earlier, a small hole was etched into the first substrate, containing the patch, to locate the feed point. This hole was transferred onto the second substrate so that the two substrates align. Once the hole was "mapped" onto the second substrate (the ground plane of the antenna), the entire square shape of the flange was cut away, leaving a square hole in the ground plane. This step was to ensure a continuous and flat ground plane for the antenna. The continuity of the ground plane was also ensured by soldering the flange of the SMA connector to the copper cladding of the ground plane. Finally, the center conductor of the probe was feed through the first substrate via the small hole and then soldered to the patch. The entire fabrication process is illustrated in Figure 25.

7.2 With Photonic Crystal in the Substrate

The fabrication of a patch with photonic crystals in the substrate followed the same procedures as discussed above, except for one modification - the insertion of the photonic crystal structure. This additional fabrication step was accomplished using a conventional hand drill. Unfortunately, at the time of manufacturing, a drill bit with a 0.5" (1.27 cm) diameter to match the crystal's hole diameter was not available. The closest bit available was a $15/32$" (1.19 cm) bit, which is roughly a 0.03" (6.25%) error in the design. However, since a hand drill was used over a conventional drill press that could have accurately placed the holes, this level of error is negligible compared to the amount of error introduced by the hand drill.

This "hand drill fabrication technique" was the cause of some serious problems in manufacturing. Since the substrate was only 50 mils thick, there was a tendency for the substrate to "bow" as the drill cut through the substrate, especially at slower drill rates. In addition, due to the small spacing between holes, problems with the substrate tearing also arose. These manufacturing problems were noted, but were set aside so that

measurements could proceed. In future generations of photonic crystal antenna, these manufacturing constraints will have to be addressed.

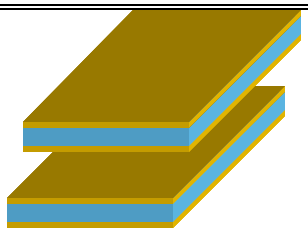	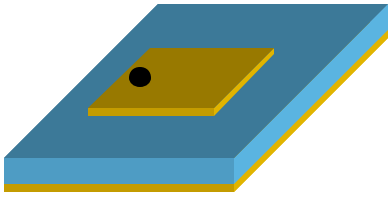	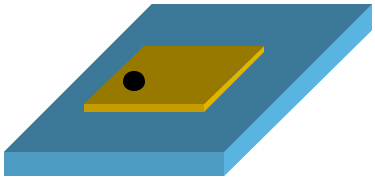
Step1: Start with two double clad substrates of roughly equal length.	Step2: Use LPKF to etch patch and drill a hole through the patch and substrate. This is the location of the feed point.	Step3: Remove bottom copper layer to establish an airgap between substrates.
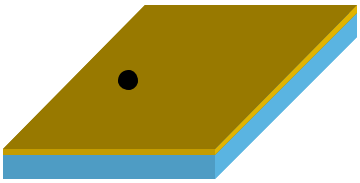	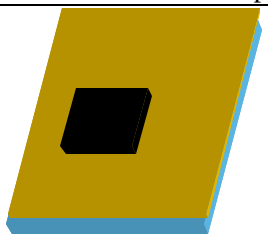	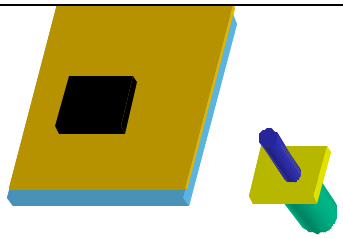
Step4: Transfer feed spot to second substrate and remove one side of copper cladding. The side shown is the ground plane for the antenna.	Step 5: Cut square hole into second substrate with the dimensions of the probe flange.	Step 6: Insert the coaxial probe through hole. This should be a snug fit.
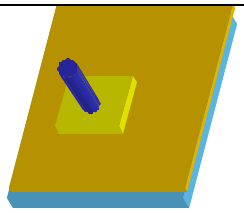	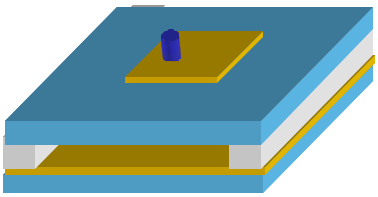	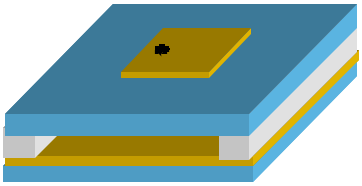
Step 7: Solder flange to copper layer to ensure a continuous ground.	Step 8: Connect substrates with Teflon screws and washers. Cut center conductor sticking above patch.	Step 9: Solder center conductor of the probe to the patch.

Figure 25. Illustration of the airgap microstrip antenna fabrication process

Chapter 8: Antenna Measurements

Verification of the analytical results obtained for the microstrip (patch) antenna with and without photonic crystals was achieved using measurement equipment at the Virginia Tech Antenna Lab.

8.1 Return Loss Measurements

The resonant frequency and bandwidth were the first data points collected on the patch antennas. These measurements were compiled using the HP-8510 Network Analyzer shown in Figure 26. Network analyzers work by measuring the magnitude and phase of the scattering parameters of a multi-port (input/output) device. For single port devices, such as patch antennas, the network analyzer needs only measure the return loss characteristics (s_{11}). The results of these measurements are shown in Figure 27 and Figure 28, illustrating the return loss in decibel plots and as Smith Charts, respectively.

As can be observed in Figure 27, the resonance points are roughly at the same frequency for both antennas, 8.87 GHz for the conventional airgap (C-AG) patch and 8.96 GHz for the photonic crystal airgap (PC-AG) patch. In both designs, the resonant frequency is different from the expected 9.5 GHz as predicted in HFSS. It is believed that this discrepancy is a direct result of tolerance issues arising from the LPKF milling station, as discussed above. It is, however, apparent that the manufacturing errors are consistent in both antenna designs. Fortunately, the bandgap of the crystal structure is large with a rejection of approximately 95% at 9.0 GHz and surface wave rejection is still expected. A detailed comparison of the C-AG patch, the PC-AG patch, and the HFSS simulated C-AG patch is tabulated in Table 2.

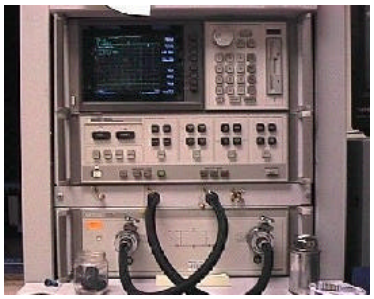

Figure 26. HP-8510 Network Analyzer at the Virginia Tech Antenna Lab used to identify the impedances and resonant frequencies for the patch designs

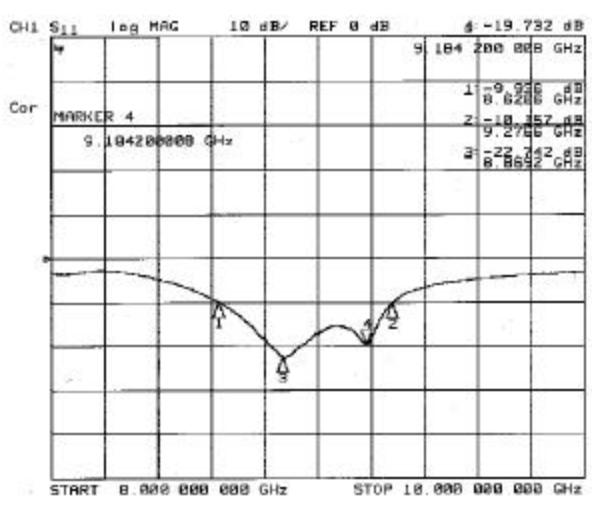

Return loss measurements of a conventional airgap (C-AG) patch antenna.

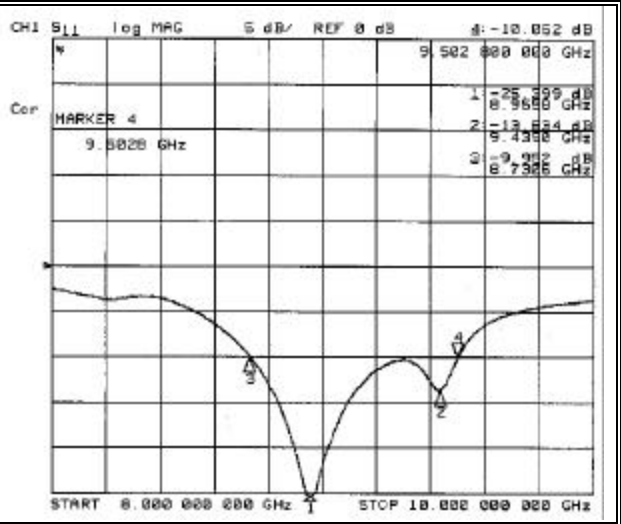

Return loss measurements for a photonic crystal airgap (PC-AG) patch antenna.

Figure 27. Return Loss measurement of C-AG patch (Left) and for the PC-AG patch (Right); illustrates bandwidth and resonance improvements

Patch Type	Resonance (GHz)	S_{11} level at resonance	10dB Bandwidth (MHz)	Bandwidth (%)
HFSS model of a C-AG (Figure 21)	9.5	-21 dB	500	5.2
Measured C-AG	8.87	-22.7 dB	650	7.3
Measured PC-AG	8.96	-25.4 dB	789.74	8.8
Agi's Design[49] (Figure 29)	9.04	-7.5 dB	NA	NA

Table 2. Tabulated comparison of the experimental and simulated results

[49] Agi and Malloy, "Integration of a Microstrip Patch Antenna with a Two-Dimensional Photonic Crystal Substrate," *Electromagnetics*, vol. 19, 1999

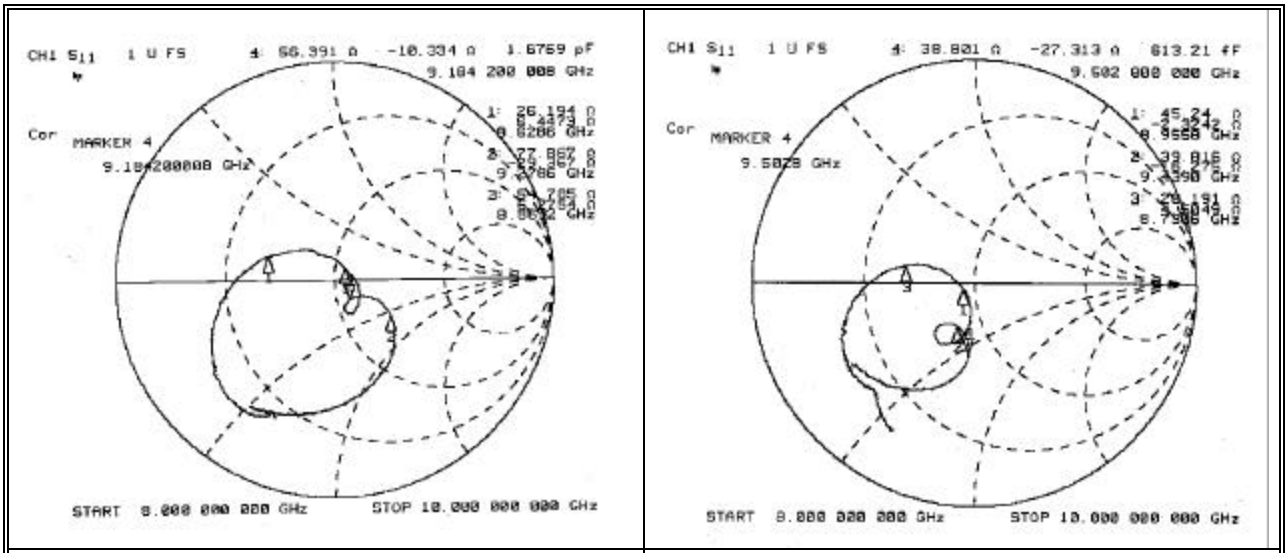

At resonance (marker 3), the C-AG antenna has nearly no reactive component as expected from the HFSS simulation, shown in Figure 22.	At resonance (marker 1), the PC-AG antenna also has nearly no reactive component.

Figure 28. Smith Chart plots for the C-AG patch (Left) and for the PC-AG patch (Right); illustrates near 50W impedances for both designs

These results illustrate two significant design improvements made possible with the introduction of the photonic crystals. First, there is almost a 3dB improvement at resonance when comparing the C-AG patch to the PC-AG patch. This is of substantial benefit when designing a communication system, since every dB improvement assists when matching the antenna and feed. In addition, improvements in signal-to-noise ratios and overall system performance are also possible. Second, there is a 1.5% increase in the 10dB bandwidth. Fundamentally, any opportunity to increase the antenna bandwidth is of substantial benefit to a communication system. This increases the potential of a system containing these antennas, since it extends its "useful" frequency spectrum.

It is obvious that the PC-AG patch is far more superior in comparison with Agi's photonic crystal patch design[50]. As shown in Figure 29, Agi's design resonates at only 7.5dB, which is impractical for use in most communication systems. Moreover, a 10dB bandwidth does not even exist. Therefore, it is concluded that the airgap dramatically improves the patch design by creating a third dimension to establish a bandgap.

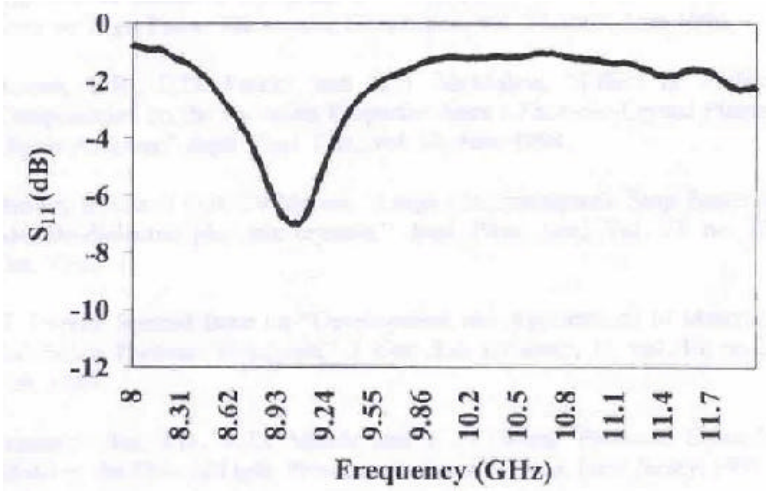

Figure 29. Return loss measurements from Agi's photonic crystal patch antenna design[51]

8.2 Anechoic Chamber Measurements

Once the resonant frequencies were identified, principal radiation patterns were taken to characterize the operational performance of each patch. These measurements were obtained using the indoor anechoic test chamber at Virginia Tech, shown in Figure 30. For these measurements, the chamber was arranged such that the source remains stationary as the antenna under test (AUT) rotates along a gimble-positioner, shown in Figure 30 (left). Principal radiation patterns consist of collinear polarization (co-pol) and

[50] Agi and Malloy, "Integration of a Microstrip Patch Antenna with a Two-Dimensional Photonic Crystal Substrate," *Electromagnetics*, vol. 19, 1999

[51] Agi and Malloy, "Integration of a Microstrip Patch Antenna with a Two-Dimensional Photonic Crystal Substrate," *Electromagnetics*, vol. 19, 1999

cross polarization (x-pol) plots, which are broken into either E-plane or H-plane cuts. The convention used in this thesis is that the orientation of the electric field lines ($\vec{E}$) of the patch defines the E-plane. Likewise, the orientation of the magnetic field lines ($\vec{H}$) of the patch defines the H-plane. For the patch designs, the electric field propagates along the XZ-plane of the patch and defines the E-plane cut, as shown in Figure 7. In a similar fashion, the YZ-plane defines the H-plane, which is perpendicular to the E-plane.

The polarization of the pattern measurement, either collinear or cross, is defined by the polarization of the source antenna. The source antenna used during experimentation was a standard X-band (8.2 – 12.4 GHz) rectangular aperture horn, shown in Figure 30 (right). Thus, to obtain an E-plane co-pol radiation pattern, the electric field ($\vec{E}$) of both antennas must align parallel (collinear) and then the positioner must rotate 360 degrees along the E-plane of the patch. E-plane x-pol is obtained by rotating the AUT 90 degrees such that the E-fields align anti-parallel, and then scanning the positioner. Likewise, H-plane co-pol is measured when the H-fields align parallel; H-plane x-pol is obtained when the H-fields align anti-parallel. Figure 31 illustrates the required antenna alignments to obtain the desired polarization measurement.

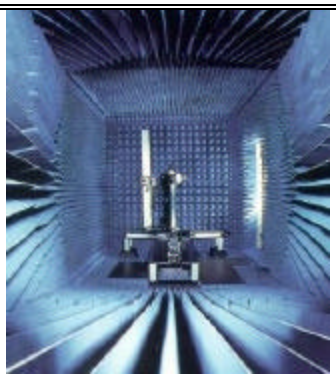	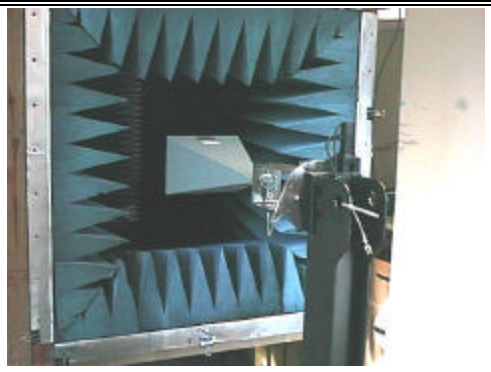
Image from the source antenna looking into the chamber and at the antenna under test (AUT).	Standard rectangular horn antenna used as the source antenna for measurements.

Figure 30. Virginia Tech indoor anaechoic test chamber used to measure antenna patterns

With the proper antenna polarization, the principal antenna patterns were measured, as illustrated in Figure 32 and Figure 33 for the E-plane and H-plane co-pol respectively. As observed in the graphs, the direction of maximum radiation is not located at boresight (θ = 0 deg) – the angle in which the line of sight the shortest. In fact, both antennas are shifted approximately 20 degrees off-boresight. This offset is also apparent in the x-pol pattern measurements, shown in Figure 34. At angle of maximum radiation, the G-AG patch displays only 2.6 dB of x-pol rejection, while the PC-AG patch exhibits 7.8 dB. The causes of these errors are believed to be the result of higher order modes, as will be discussed in the next section.

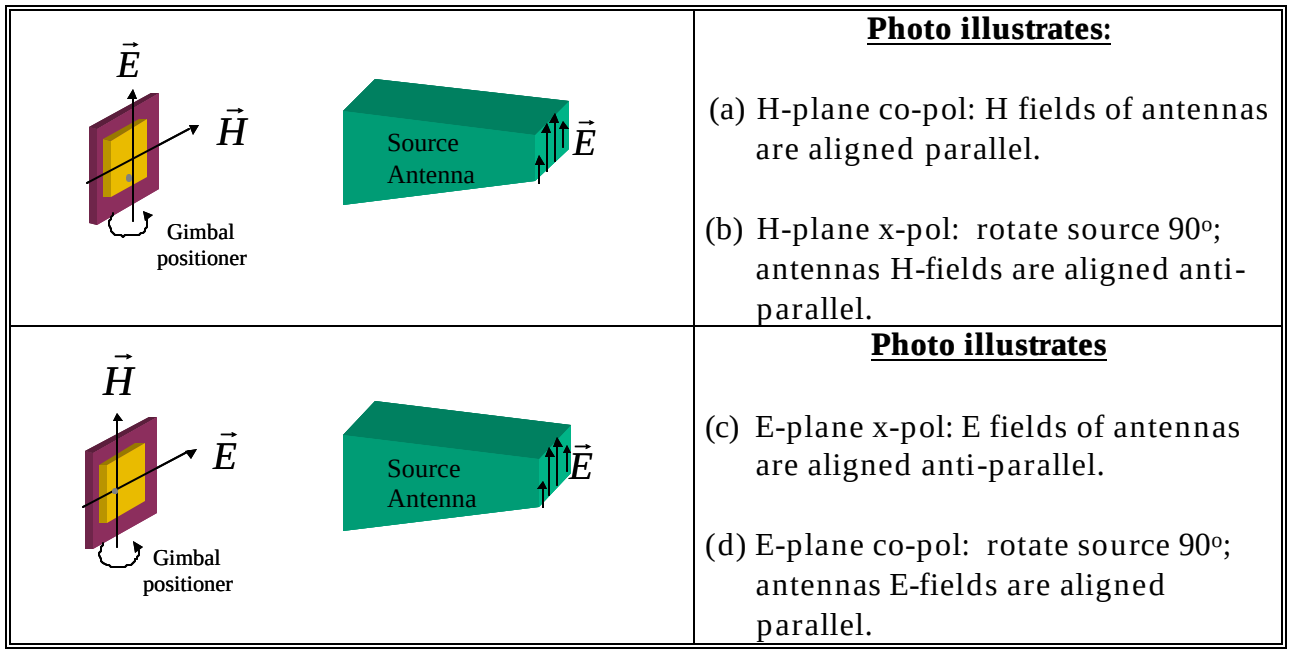

Photo illustrates:

(a) H-plane co-pol: H fields of antennas are aligned parallel.

(b) H-plane x-pol: rotate source 90°; antennas H-fields are aligned anti-parallel.

Photo illustrates

(c) E-plane x-pol: E fields of antennas are aligned anti-parallel.

(d) E-plane co-pol: rotate source 90°; antennas E-fields are aligned parallel.

Figure 31. Alignment of the AUT and source to obtain desired polarization measurements

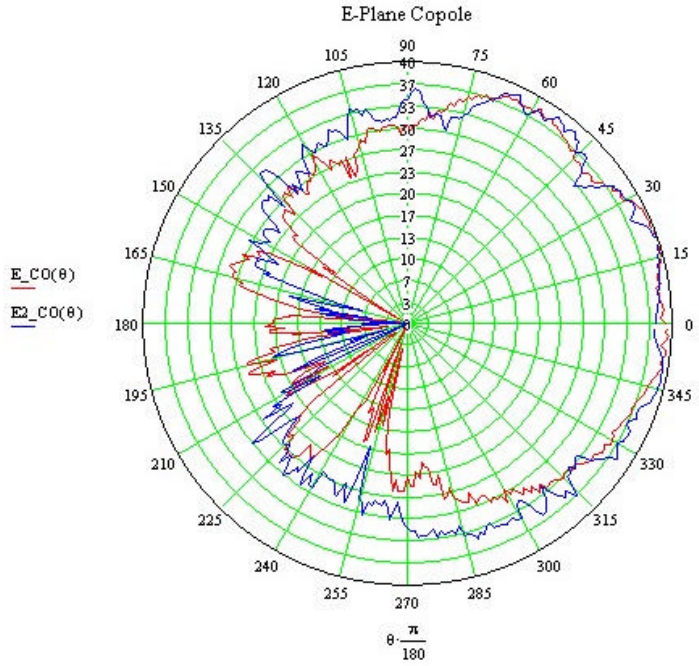

Figure 32. Comparison of the E-plane co-pol antenna patterns (Blue: C-AG patch and Red: PC-AG patch)

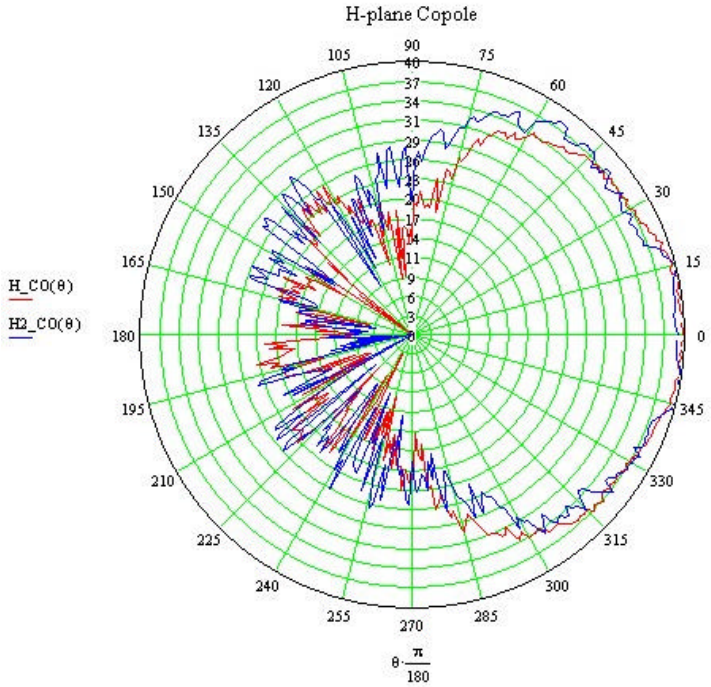

Figure 33. Comparison of the H-plane co-pol antenna patterns (Blue: C-AG patch and Red: PC-AG patch)

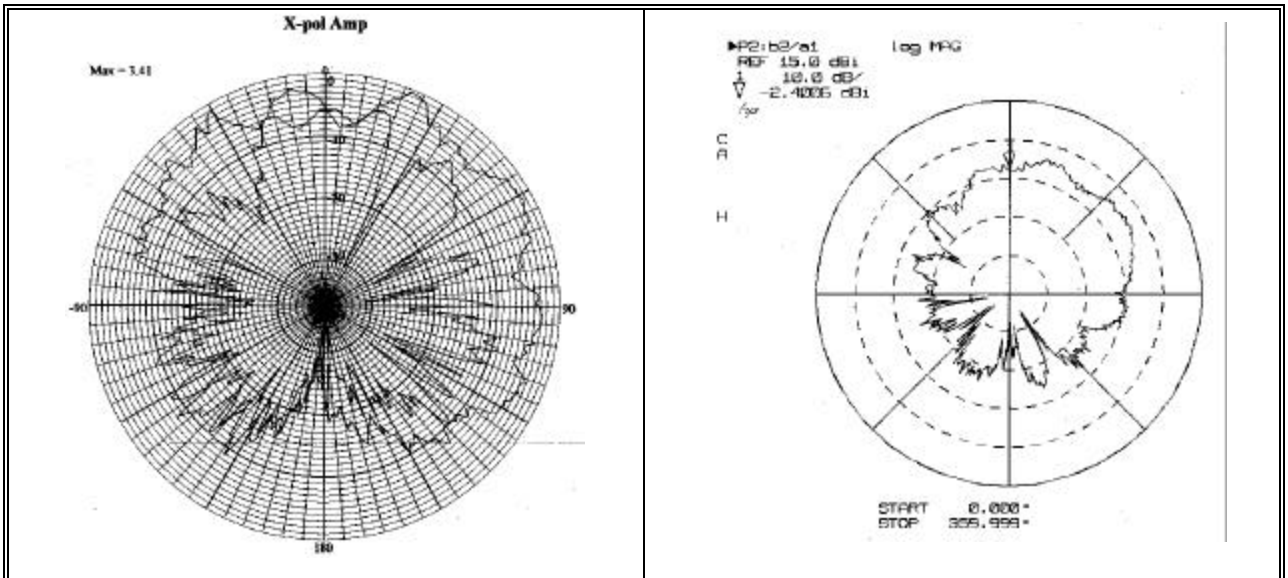

E-plane X-pol measurements for the C-AG patch	E-plane X-pol measurement for the PC-AG patch

Figure 34. Comparison of the X-pol antenna patterns for the C-AG patch (Left) and the PC-AG patch (Right)

Despite the evident design error, there is still some valuable information obtainable from these measurements. First, an estimation of directivity is obtainable by evaluating the half power beamwidths (HPBW) of the principal radiation patterns. Using the co-pol radiation plots, the HP points were determined by locating the angle of maximum illumination and then locating the angles associated with an E-field intensity that is 3dB less or half-power. For the C-AG antenna, the measured HPBWs were 58^{o} for both principal co-pol cuts. For the PC-AG antenna, the HPBWs were 52^{o} and 59^{o}, for the E-plane and H-plane co-pol cut respectively. Based on these values, an approximate directivity can be calculated using equation (32)[52]. The result is that the PC-AG antenna is more directive (D = 10.3 dB) than the C-AG antenna (D = 9.8 dB). In fact, the PC-AG patch is even more directive than Agi's thin substrate design[53], where a nearly omni-directional patch pattern was obtained with HPBWs of 70.0^{o} for both principal

[52] Stutzman and Thiele, *Antenna Theory and Design*, 2nd ed: John Wiley & Sons, Inc., 1998.
[53] Agi and Malloy, "Integration of a Microstrip Patch Antenna with a Two-Dimensional Photonic Crystal Substrate," *Electromagnetics*, vol. 19, 1999

patterns and a directivity of 8.2 dB. This tends to indicate that the third dimension of the bandgap also improved the radiation patterns of the patch antennas. Measured results and calculations are summarized in Table 3.

$$D = \frac{32000}{HP_E HP_H} \tag{32}$$

Patch Type	Pattern Max. (degrees)	HPBW (E-plane)	HPBW (H-plane)	Directivity (dB)	F/B Ratio (E-plane) (dB)	F/B Ratio (H-plane) (dB)
C-AG	18	58.0	58.0	9.8	7.0	11.0
PC-AG	20	52.0	59.0	10.3	10.0	15.0
Agi's Design	0	70.0	70.0	8.2	13.0	13.0

Table 3. Tabulated results obtained from anechoic chamber measurements for the C-AG and PC-AG patches and from Agi's design

Another significant result is the noticeable reduction in sidelobe level in both principal co-pol radiation patterns. At certain scan angles, the photonic crystal appears to drop sidelobe levels as low as 15dB when compared to the C-AG antenna. This is a dramatic improvement in performance! This illustrates the photonic crystal's ability to suppress sidelobes by reducing surface waves. In other words, the radiation of the edge of the substrate becomes suppressed such that more energy is transmitted through the antenna's mainbeam, oppose to in the sidelobes.

In addition, by suppressing the sidelobe levels, the front-to-back (F/B) ratios of the antennas are also improved. As shown in Table 3, a 3-4 dB improvement is obtained when inserting the photonic crystal into the substrate of a C-AG patch. These results are comparable to Agi's results, illustrating that the third dimension of the bandgap does not dramatically improve F/B ratios as compared to a 2D photonic crystal.

In summary, utilizing photonic crystals in a patch antenna with an airgap appears to perform four key functions:

(1) Increase operation bandwidth
(2) Reduce sidelobe levels
(3) Reduced F/B ratios
(4) Increase directivity

8.3 Additional Explanation of Results

To identify the reasoning behind the off-boresight antenna patterns exhibited in both patch antennas, detailed investigations on the design methodology were performed. The most suspicious parameter in the design was the placement of the feed. Recall from Figure 21, the probe was offset by 0.6 mm with respect to the y = 0 plane to obtain the deepest resonance in the return loss graph (Figure 22). It is strongly believed that this offset resulted in the excitation of higher order modes and the beginning of circular polarization, which in turn resulted in an off-boresight radiation and higher than expect x-pol patterns. This hypothesis was confirmed using HFSS.

As experience using HFSS improved, it was discovered that HFSS is capable of determining the EM field lines and radiation pattern of an antenna to compliment the return loss measurements. As shown in Figure 35, HFSS agrees with the experimental radiation pattern results (Figures 32 – 34), illustrating that the C-AG patch antenna, in fact, radiate with an off-boresight pattern. This was a fundamental flaw in my design, in that the design was focused on establishing a perfect match between the antenna and feeds. Using this approach, pattern polarization and operating mode are ignored, leading to the apparent excitation of higher order modes and circular polarization.

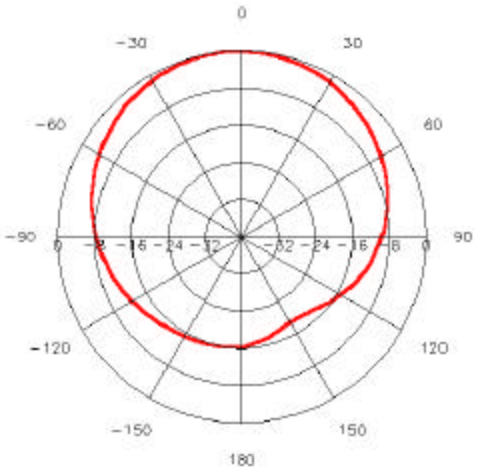

Figure 35. E-Plane Co-pol. pattern as predicted in HFSS demonstrating a similar 18-degree off-boresight pattern

Upon further investigation, HFSS also verified that the patch is indeed operating in an undesired mode. Instead of operating in the dominant TM_{010} mode, the field from the patch radiate as if operating with a TM_{110} mode. This was determined by observing how the E-fields radiate on the surface of the patch. As illustrated in Figure 36, the field lines radiate off the corners of the substrate oppose to the flat edges for radiation with in a TM_{010} mode. This field line orientation is a classical exhibition of a patch operating in a TM_{110} mode[54], which is favorable for circular polarization. This explains the unusually large x-pol pattern that is uncommon for linear polarized antennas.

[54] Gupta and Benalla, *Microstrip Antenna Design*: Artech House, 1988.

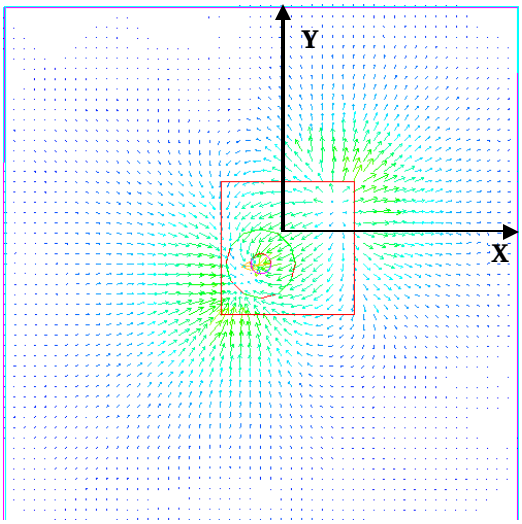

Figure 36. Illustration of E-field when the probe is offset from the centerline of the patch. The green lines show the highest intensity of the fields

8.4 Recalculation of the Design

In order to establish linear polarization in the principal radiation patterns, a second-generation G-AG patch was designed using HFSS. Initially, the dimensions of this patch and the airgap spacing remained constant; adjustments were made only on the point of excitation (feed position). To ensure the propagation of the dominant TM_{010} mode, the excitation point was set with a zero-offset along the y-axis, as illustrated in Figure 37. By placing the feed at this point, symmetry is established along the XZ-plane of the patch, focrcing the E-field lines to radiate off the flat edges patch, oppose to the corners. This arrangement excites the dominant TM_{010} mode, as shown in Figure 38.

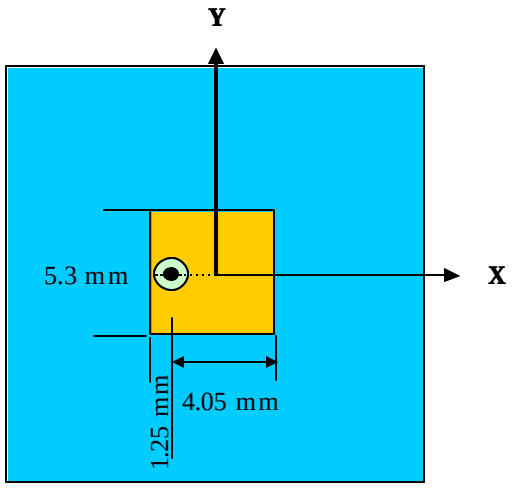

Figure 37. Final dimensions for the modified C-AG patch design that would ensure linear polarization and reduce the x-pol patterns

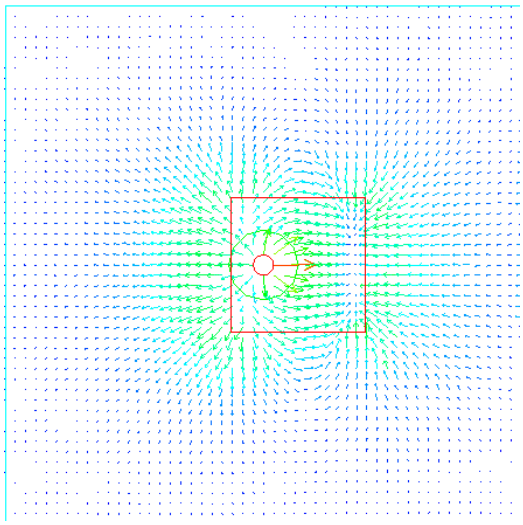

Figure 38. Illustration of E-field when the probe is placed on the centerline of the patch. The green lines show the highest intensity of the fields

Once the operating mode was identified, the resonant frequency of the patch was analytically evaluated, using HFSS. As illustrated in Figure 39 (left), with the new feed location, the C-AG patch resonates at 9.7 GHz, instead of the desired 9.5 GHz. To "scale down" the frequency, the dimensions of the square patch were increased from the original 5.2x5.2 mm^2 to 5.3x5.3 mm^2 - increasing the size of the antenna decreases the

resonant frequency[55]. This increase in patch size reduced the resonant frequency to 9.5 GHz with 35 dB of rejection at resonance. A 10dB bandwidth of 600MHz (6.3%) was also calculated.

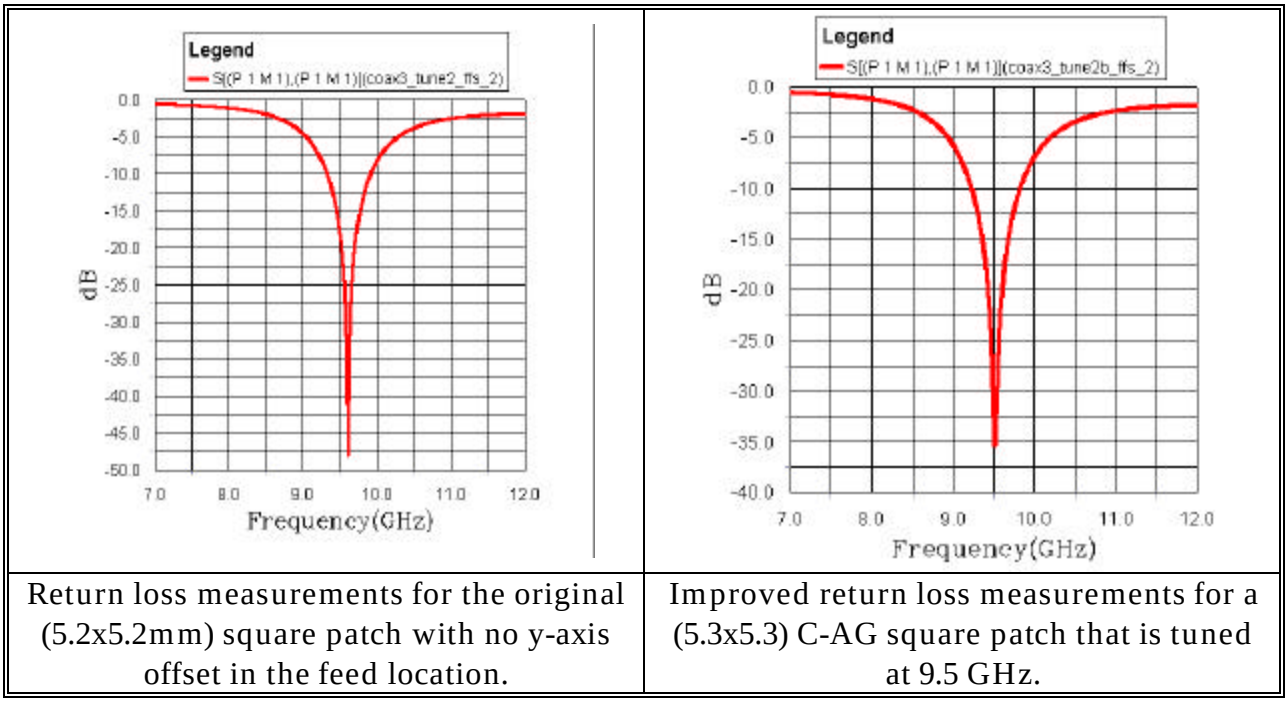

Return loss measurements for the original (5.2x5.2mm) square patch with no y-axis offset in the feed location.	Improved return loss measurements for a (5.3x5.3) C-AG square patch that is tuned at 9.5 GHz.

Figure 39. HFSS simulated return loss measurements for the re-design C-AG patch; (Left) illustrates design with original patch dimensions; (Right) Illustrates design with new patch dimensions

Finally, the radiation patterns for the newly designed patch were evaluated using HFSS. The software shows that with the new dimensions of the patch and new excitation point, the antenna is now linearly polarized and radiates at boresight ($\theta = 0^o$). This is confirmed by reviewing the E-plane principal co-pol and x-pol radiation patterns, as shown in Figure 40. The overlaid plot of the co-pol pattern (green) illustrates boresight radiation at $\theta = 0^o$, while the x-pol pattern (blue) is nearly 20 dB down from the peak. The lower x-pol component verifies that most of the antenna's power radiates in the

[55] Pozar and Schaubert, *Microstrip Antenna: The Analysis and Design of Microstrip Antennas and Arrays*: IEEE Press, 1995.

main beam and not in erroneous higher order modes. Thus, linear polarization is confirmed.

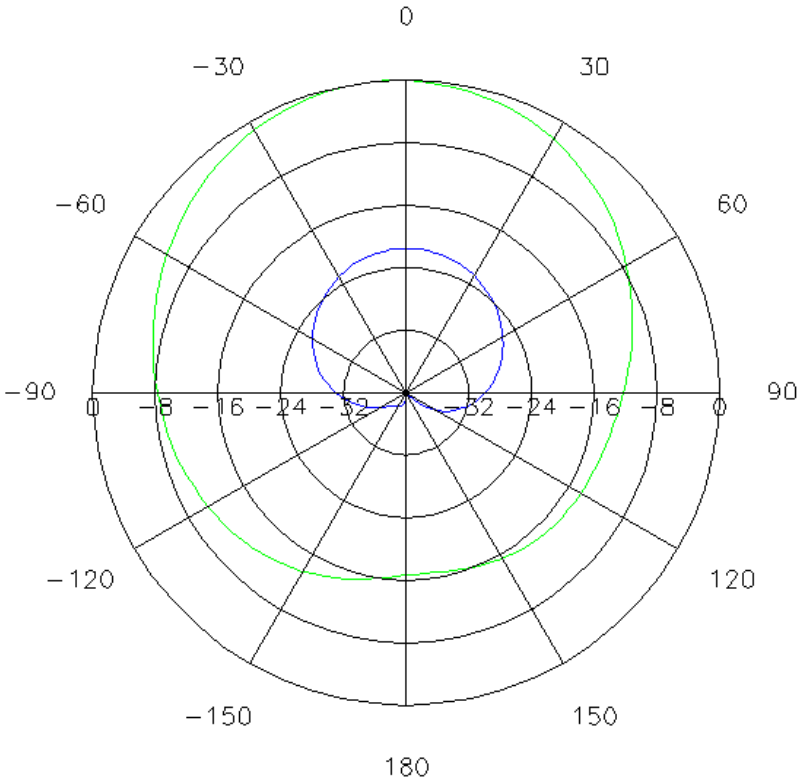

Figure 40. HFSS simulated E-Plane Co-pol. pattern and X-pol patterns; Note that the antenna points at boresight (q = 0)

Chapter 9: Conclusion

This thesis introduced and investigated a novel concept in the development of wideband microstrip antennas using photonic crystals. Photonic crystals were realized to reduce and, in some cases, eliminate surface waves, which leads to an increase in directivity, bandwidth, front-to-back ratios, and efficiency, all while reducing pattern sidelobe levels. The concept of introducing an airgap to separate the dielectric and ground plane has proven to be effective in improving the radiation characteristics of a photonic crystal based antenna designed on a thin substrate.

With the airgap in the conventional airgap (C-AG) and photonic crystal airgap (PC-AG) patch, promising results were obtained from the experiments. First, the photonic crystal lattice improved the bandwidth of a C-AG patch from 7.3% to 8.8%, improved directivity from 9.8 dB to 10.3 dB, and reduced sidelobe levels in certain areas by more than 10dB. In addition, in comparison study with another thin substrate photonic crystal approach the novel airgap design proved to demonstrate higher performance.

In the future, investigations into determining methods to minimize the surface area consumed by the photonic crystal lattice are required. To obtain nearly 98% reflection from the bandgap requires four periods of the crystal geometry, consuming nearly all the surface of the substrate. Suggested methods to remedying this issue include (1) reducing the diameter of the hole while increasing the number of holes in the substrate and (2) changing the geometry of the array grid from triangle to a square, for example.

Bibliography

[1] E. R. Brown and O. B. McMahon, "Large Electromagnetic Stop Bands in Metallo-dielectric photonic crystals," *Applied Physics Letter*, vol. 67, 1995.

[2] W. Stutzman and G. Thiele, *Antenna Theory and Design*, 2nd ed: John Wiley & Sons, Inc., 1998.

[3] D. Pozar and D. Schaubert, "Microstrip Antennas," *Proceedings of the IEEE*, vol. 80, 1992.

[4] C. Balanis, *Antenna Theory Analysis and Design*, 2nd ed: John Wiley & Sons, Inc., 1997.

[5] E. R. Brown and C. D. Parker, "Radiation Properties of a Planar Antenna on a Photonic-Crystal Substrate," *J Opt Soc Am B*, vol. 10, 1993.

[6] D. Pozar and D. Schaubert, *Microstrip Antenna: The Analysis and Design of Microstrip Antennas and Arrays*: IEEE Press, 1995.

[7] K. Agi and J. Malloy, "Integration of a Microstrip Patch Antenna with a Two-Dimensional Photonic Crystal Substrate," *Electromagnetics*, vol. 19, 1999.

[8] G. Parker and M. Charlton, "Photonic Crystals," *Physics World*, 2000.

[9] R. Gonzalo and B. Martinez, "The Effect of Dielectric Permittivity on the Properties of Photonic Band Gap Devices," *Microwave and Optical Technology Letters*, vol. 23, 1999.

[10] V. Radisic and Y. Qian, "Novel 2-D Photonic Bandgap Structure for Microstrip Lines," *IEEE Microwave and Guided Wave Letters*, vol. 8, 1998.

[11] R. D. Meade, A. M. Rappe, K. D. Brommer, and J. D. Joannopoulos, "Nature of the photonic bandgap: some insights from field analysis," *J Opt Soc Am B*, vol. 10, pp. 328-332, 1993.

[12] R. Gonzalo, "Enhanced Patch-Antenna Performance by Suppressing Surface Waves Using Photonic-Bandgap Substrates," *IEEE Transaction on Microwave Theory and Techniques*, vol. 47, 1999.

[13] R. Coccioli, W. R. Deal, and T. Itoh, "Radiation Characteristics of a Patch Antenna on a Thin PBG Substrate," *IEEE Transaction on Antennas and Propagation*, vol. 45, pp. 656-659, 1998.

[14] J. S. Dahrele and Lee, "Theory and experiment on microstrip antennas with air gaps," *IEE Proceeding Microwave and Antenna Propagation*, vol. 132, 1985.

[15] D. Pozar, *Microwave Engineering*, 2nd ed: John Wiley & Sons, Inc., 1998.

[16] Abboud, Damiano, and Papiernik, "Accurate Model for the input impedance of coax-fed rectangular microstrip antenna with and without airgaps," *Proceedings of the IEEE*, vol. 135.

[17] K. C. Gupta and A. Benalla, *Microstrip Antenna Design*: Artech House, 1988.

Vita

Keith Huie was born in Washington, DC on November 2, 1975. He received a B.S.E.E. degree from the University of Pittsburgh in May 1997. For 3 years after graduation, he was employed by Raytheon Company designing and testing antennas and high frequency electronic systems for military and commercial applications. In December 2000, he joined the Virginia Tech Fiber and Electro-Optics Research Center. He is currently pursuing a Ph.D. in electrical engineering at Virginia Tech under the tutelage of Dr. Richard Claus.